Integrin Structure, Allostery, and Bidirectional Signaling

M.A. Arnaout, B. Mahalingam, and J.-P. Xiong

Structural Biology Program, Leukocyte Biology and Inflammation Program, Nephrology Division, Department of Medicine, Massachusetts General Hospital and Harvard Medical School, Charlestown, Massachussetts 02129; email: arnaout@receptor.mgh.harvard.edu, bmahalingam@partners.org, xiong@helix.mgh.harvard.edu

Annu. Rev. Cell Dev. Biol. 2005. 21:381–410

First published online as a Review in Advance on June 28, 2005

The *Annual Review of Cell and Developmental Biology* is online at http://cellbio.annualreviews.org

doi: 10.1146/annurev.cellbio.21.090704.151217

1081-0706/05/1110-0381$20.00

Key Words

cell adhesion, inflammation, cancer, hemostasis, therapeutics

Abstract

$\alpha\beta$ heterodimeric integrins mediate dynamic adhesive cell-cell and cell-extracellular matrix (ECM) interactions in metazoa that are critical in growth and development, hemostasis, and host defense. A central feature of these receptors is their capacity to change rapidly and reversibly their adhesive functions by modulating their ligand-binding affinity. This is normally achieved through interactions of the short cytoplasmic integrin tails with intracellular proteins, which trigger restructuring of the ligand-binding site through long-range conformational changes in the ectodomain. Ligand binding in turn elicits conformational changes that are transmitted back to the cell to regulate diverse responses. The publication of the integrin $\alpha V\beta 3$ crystal structure has provided the context for interpreting decades-old biochemical studies. Newer NMR, crystallographic, and EM data, reviewed here, are providing a better picture of the dynamic integrin structure and the allosteric changes that guide its diverse functions.

Contents

INTRODUCTION

Cells exist in a highly dynamic extracellular milieu consisting of complex chemicals and mechanical stress signals to which cells must continuously adjust and in turn modulate. In metazoa, the task of integrating these mechanochemical cues across the plasma membrane is mediated mainly by integrins: heterodimeric cell surface glycoproteins comprised of α- and β-subunits each spanning the plasma membrane once. Since the identification of this receptor family more than two decades ago, intensive efforts have been made to understand its complex functions as mechanochemical sensors and transducers. More recent studies have focused on elucidating the underlying structure-activity relationships in order to understand the regulatory roles of these receptors in cellular function. Since integrins also participate in injury and disease, a potential outcome is the discovery of small molecule antagonists to treat common diseases linked to integrin dysfunction such as cancer, thrombosis, and chronic inflammation. Here, we review these new structural advances, placing them in the biologic context.

vWFA: von Willebrand Factor type A

THE INTEGRIN FAMILY

In mammals, 24 integrins have been identified to date, resulting from different pairings among 18 α- and 8 β-subunits. The extracellular segment of the α- and β-subunits has up to 1104 residues and 778 residues respectively, with the N-terminal portions of each subunit combining to form a globular ligand-binding "head" connected to the membrane by a long (~170 Å) stalk. One-half of the mammalian α-subunits contain an additional ~190 amino acid vWFA domain (αA, also known as I domain); nine integrins belong to this αA-containing subclass.

Integrins recognize a large number of physiologic ligands, including soluble and surface-bound proteins. Unlike binding to soluble ligands, integrin binding to ligands on rigid surfaces results in force generation at the focal contacts (meeting points of the integrin with ligand), which directly affects the cell's contractile apparatus and is a key element in the assembly and remodeling of the extracellular matrix (Ingber 2003, Ridley 2004). Integrin binding to ligands requires divalent cations and invariably involves a

solvent-exposed aspartate or a glutamate (in the case of the αA-containing subclass) from the ligand. High-affinity binding of αA-lacking or -containing integrins to physiologic ligands is not constitutive but requires a conformational switch of the ligand-binding site. This regulatory mechanism allows leukocytes and platelets, for example, to circulate in the blood without pathologically adhering to each other or to the vascular wall. The switch to the high-affinity state is rapid, with a subsecond time frame, is reversible in less than a minute, and is triggered from within the cell (hence the term inside-out activation) in response to extracellular chemical (Constantin et al. 2000, Lollo et al. 1993) and/or mechanical stress signals (Zwartz et al. 2004b). The intracellular activation signals are channeled through the short integrin cytoplasmic and transmembrane segments to the extracellular ligand-binding pocket. Many integrins [e.g., αMβ2 (CD11b/CD18) or αIIbβ3] exist in two activation states (active and inactive) (Litvinov et al. 2002, Xiong et al. 2000), while some [e.g., α4β1 (Chigaev et al. 2001)] may also display intermediate-affinity states. Integrins bound to soluble or immobilized physiologic ligands form micro- (tens of angstroms scale) or macro- (tens of nanometer scale) clusters (Kim et al. 2004) and transmit mechanochemical signals inwards (outside-in signaling) that reorganize the cytoskeleton; in this way, integrins modulate much of the cell's metabolic and signal transduction machinery (Ingber 2003, Schwartz & Ginsberg 2002).

The inside-out–driven change in integrin affinity occurs primarily through a 30–100-fold reduction in the dissociation rate, with a smaller contribution from the increased association rate, implying that conformation of the ligand-binding pocket rather than its accessibility on the cell surface is the main contributor to stimulus-induced affinity switching (Zwartz et al. 2004a). The dissociation rates of high-affinity integrins (0.02–0.2 s^{-1}) responsible for firm adhesion are typically an order of magnitude less than those of selectins (Bhatia et al. 2003). The high dissociation rates (~2.6–4.6 s^{-1}) (Shimaoka et al. 2003b, Smith et al. 1999) of the low- and intermediate-affinity states allow some integrins (e.g., α4 integrins) to mediate cell rolling, like selectins. Thus depending on their affinity state, such integrins may mediate rolling or firm adhesion.

MIDAS: metal ion-dependent adhesion site

THE ALPHA SUBUNIT vWFA DOMAIN (αA)

Conformational States of αA

In 1995, the first crystal structure of the integrin αA domain was published (Lee et al. 1995b), soon after it was demonstrated that this domain is the major ligand-binding site in αA-containing integrins (Michishita et al. 1993). The globular αA is composed of a GTPase-like domain, in which the catalytic center on the domain's upper surface is replaced with an invariant ligand-binding site named MIDAS. Isolated αA domains exist in two conformations—closed and open (**Figure 1**)—which equate respectively with the low- and high-affinity ligand-binding states of the domain (Emsley et al. 2000, Lee et al. 1995a,b, Li et al. 1998, Shimaoka et al. 2003b, Xiong et al. 2000). In the closed state, a metal ion (Mn^{2+}) is coordinated by a D140xSxS MIDAS motif from the βA-α1 loop (loop 1, x for any amino acid, residue numbering is from CD11b), a T209 from the α3-α4 loop (loop 2) that hydrogen bonds to a metal-bound water, and a D242 from the βD-α5 loop (loop 3) that directly coordinates the metal ion producing the Thr-water-metal-Asp closed MIDAS configuration. A water molecule completes the octahedral coordination sphere around the metal. In all closed αA structures, the βF-α7 (F-α7) loop occupies an identical position, stabilized by hydrophobic contacts with the central β-sheet, but the C-terminal α7 helix is not always packed against the central strand. In the αA structure from CD11a, this helix is flexible following its first helical turn (Qu &

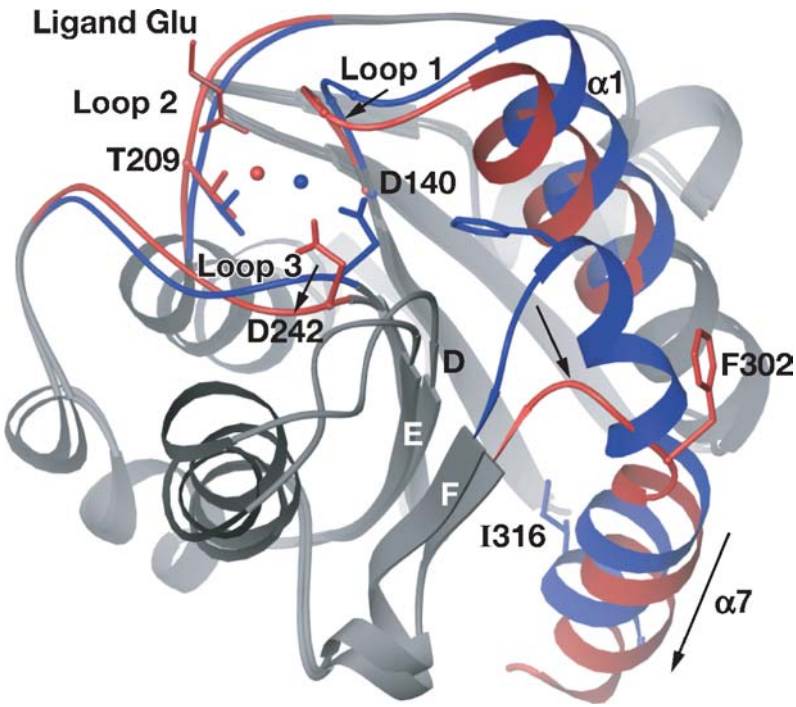

Figure 1

Structures of closed and open αA from integrin CD11b. Ribbon diagram of the crystal structures of open and closed αA from integrin CD11b. Major conformational differences are shown in red (*open*) and blue (*closed*), with the MIDAS metal shown in the respective color. The ligand Glu is in red and the MIDAS residues T209, D242, and the D140xSxS motif are indicated (for clarity, only the side chains for the first two are shown). Arrows indicate direction of major movements. This figure and the subsequent figures are made using Ribbons (Carson 1987).

Leahy 1995, 1996), perhaps as a function of the construct and/or crystal packing.

All three MIDAS loops rearrange as the domain switches to the open state (**Figure 1**). This appears to be driven by a major restructuring of the F-α7 loop and is associated with a downward two-turn displacement of the α7 helix. The rearranged contacts of the F-α7 loop with the hydrophobic core lead to a 2 Å inward pull of the α1 helix, resulting in the open MIDAS configuration Thr-metal-water-Asp. This change is linked to a 2 Å inward movement loop 1 (bearing the MIDAS motif) and in position of loop 3 bearing D242 that allows T209 to coordinate directly the metal ion (Mg^{2+} or Mn^{2+}) while D242 hydrogen bonds to a metal-bound water molecule. The resulting increased electrophilicity of MIDAS permits a glutamate from the ligand to provide the sixth metal coordination, replacing a water molecule. This restructuring of MIDAS also results in a ten fold enthalpy-driven increase (from mM to ~0.1 mM) in affinity of MIDAS to the proadhesive physiologic cation Mg^{2+} approaching that of Mn^{2+} (~0.03 mM), whose affinity remains unchanged in both conformations. Activation of αA does not alter the low (>1 mM) affinity of this domain to the generally inhibitory Ca^{2+} (Ajroud et al. 2004). Atomic force microscopy (AFM) measurements of the rupture forces of the cell-bound αA-integrin CD11a/CD18 from its surface-immobilized ligand were 20–320 pN at a loading rate of 0.02–50 nN s^{-1} (Zhang et al. 2002), revealing inner and outer activation barriers. The inner

steep barrier probably reflects the ionic interaction between the ligand glutamate and the MIDAS ion; this interaction allows the complex to resist large pulling forces. The outer barrier is likely explained by the high-affinity determining tertiary changes in the structure.

Engineering Open Forms of αA

Stable open forms of αA have been produced by locking the F-α7 segment into the open conformation. A first approach was to break the α7 helix by substituting an invariant I316 (in CD11b, **Figure 1**) with glycine (Xiong et al. 2000). In the closed state, Ile316 is buried into a hydrophobic socket (socket for isoleucine or SILEN), linking the lower part of α7 to the central sheet of the CD11b and CD11c αA domains, but is displaced from this socket by the downward displacement of α7 (Vorup-Jensen et al. 2003, Xiong et al. 2000). The expressed domain assumed the open conformation, was of high affinity even in the context of the whole integrin, and exhibited a distinctive mAb-binding profile in solution (Xiong et al. 2000) and a 2 Å increase in its hydrodynamic Stokes radius (Vorup-Jensen et al. 2003). Engineered disulfides (based on the open structure of CD11b) targeting the N-terminal region of the α7 helix (Shimaoka et al. 2003b) or Lys315 of CD11b (McCleverty & Liddington 2003) yielded open but unliganded high-affinity αA domains (K_d ~200–600 nM) that mirror the high-affinity state of the respective active parent integrin.

Mapping studies have identified the residues on the MIDAS face involved in αA binding to physiologic ligands (Li et al. 1998, Zhang & Plow 1999). These residues derive from the three conformationally sensitive MIDAS loops and encircle the MIDAS metal. More recently, crystal structure determination of αA domains in complex with certain physiologic ligands, i.e., a collagen peptide and CD54 (ICAM-1), defined the integrin-ligand interface in atomic detail and identified some of the very same MIDAS loop residues identified earlier as directly contacting the ligand (Emsley et al. 2000, Shimaoka et al. 2003b). The F-α7 loop does not contribute directly to the αA-ligand interface but affects it allosterically. In liganded αA structures, the position of the F-α7 loop is almost superimposable, despite the C-terminal α7 helix's highly variable conformation, which is dictated by the disulfides used to lock open the domain (**Figure 2**). These findings suggest that rearrangement of the F-α7 loop in αA domains, normally through the axial downward

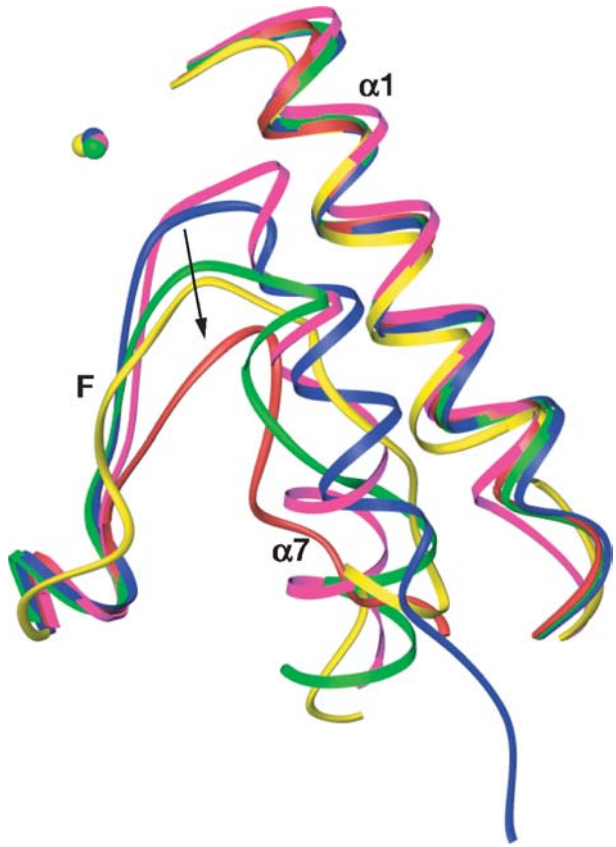

Figure 2

Structures of wild-type and mutant forms of closed and open αA domains in the F-α7 region. Ribbon diagrams of the F-α7 and α1 helix and MIDAS metal were superimposed using TOP (Lu 2000) from the crystal structures of the closed wild-type αA of CD11b (*magenta*) and the closed wild-type (*blue*), unliganded (*green*), and liganded (*yellow*) intermediate-affinity forms and the unliganded high-affinity form (*red*), all from CD11a. The MIDAS ion is colored accordingly, except for the unliganded high-affinity form, where no MIDAS metal is present in the structure (Shimaoka et al. 2003b). The arrow indicates direction of major movements in the F-α7 loop.

displacement of the α7 helix or artificially by mutations, is the critical component in induction of the high-affinity state.

PSI domain: plexin-semaphorin-integrin domain

αA Antagonists

Although the high-affinity binding of physiologic ligands to αA-integrins is activation-dependent (i.e., requires the open state), nonphysiologic ligands that function as competitive antagonists bind with nM affinity to closed αA domains expressed either alone or in the context of the whole integrin. Examples include the hookworm-derived neutrophil inhibitory factor (Rieu et al. 1996), mAb 107 (Li et al. 2002b), and mAb AQC2 (Karpusas et al. 2003). A recent crystal structure of αA from integrin α1β1 in complex with AQC2 Fab (Karpusas et al. 2003) revealed that a ligand Asp (instead of the Glu provided by physiologic ligands) completes the MIDAS coordination sphere, which assumes the open MIDAS configuration, yet the structure adopts the closed state (i.e., it lacks the associated protein movements in the F-α7 loop and α7 helix) (**Figure 3*a***). Thus, with ligand-mimetic antagonists, induction of the open MIDAS configuration does not trigger the conformational changes in the F-α7 axis at the base of the structure. This may be explained by a tighter interface or by additional contacts that prevent such movements, "freezing" the domain in the closed state.

A second class of αA antagonists acts noncompetitively to lock the domain in the inactive state. These antagonists act by stabilizing the hydrophobic contact between the α7 helix and the central β-sheet (**Figure 3*b***). The prototype of this group is lovastatin, identified using a chemical library screening approach (Kallen et al. 1999). Lovastatin wedges itself in a large hydrophobic pocket, IDAS (I domain allosteric site), between the central sheet and the α7 helix of CD11a (Kallen et al. 1999); IDAS is equivalent to SILEN in CD11b (Xiong et al. 2000). The lovastatin binding pocket is present in one structure of isolated closed αA of CD11a (Qu & Leahy 1995) but not another (generated in the absence of metal ions (Qu & Leahy 1996), but is readily accessible in native CD11a/CD18 (Kallen et al. 1999, Weitz-Schmidt et al. 2004). Additionally, mutations of the invariant I316 equivalent in CD11a are activating in the native integrin but not in isolated αA (Lupher et al. 2001; Li and Arnaout, unpublished data). These findings again suggest that flexibility of the CD11a α7 helix seen in closed recombinant αA is not reflective of the normal position of this helix in the native inactive form of this integrin.

STRUCTURE OF THE INTEGRIN ECTODOMAIN

Integrin Domains and Quaternary Structure

The crystal structure of the unliganded ectodomain from the αA-lacking integrin αVβ3 was determined in the presence of Ca^{2+} and Mn^{2+} (Xiong et al. 2001, 2002, 2004). It revealed 12 domains: four in the αV-subunit and eight in the β3-subunit (**Figure 4*a*,*b***). The two subunits assemble into a globular head built by two predicted domains: an N-terminal seven-bladed β-propeller domain of αV (Springer 1997) and an αA-like domain (βA) from β3 (Lee et al. 1995b). βA loops out from an Ig-like "hybrid" domain (β3 residues 55–108 and 353–432), which itself is inserted in the N-terminal PSI domain (residues 1–54 and residues 433–435) of β3. The PSI domain is followed by four EGF-like domains (of which EGF1 and 2 are poorly visible in the electron density map) and a novel membrane-proximal β-tail domain (βTD), all together forming the β3 leg. The corresponding αV leg is formed of an Ig-like thigh domain followed by two large β-sandwich domains, calf-1 and calf-2, the latter containing the proteolytic cleavage site that results in the heavy and light chains of αV upon reduction. An unexpected feature of the structure (Xiong et al. 2001) is that the legs are bent at the "knees" and folded back against the head of the same

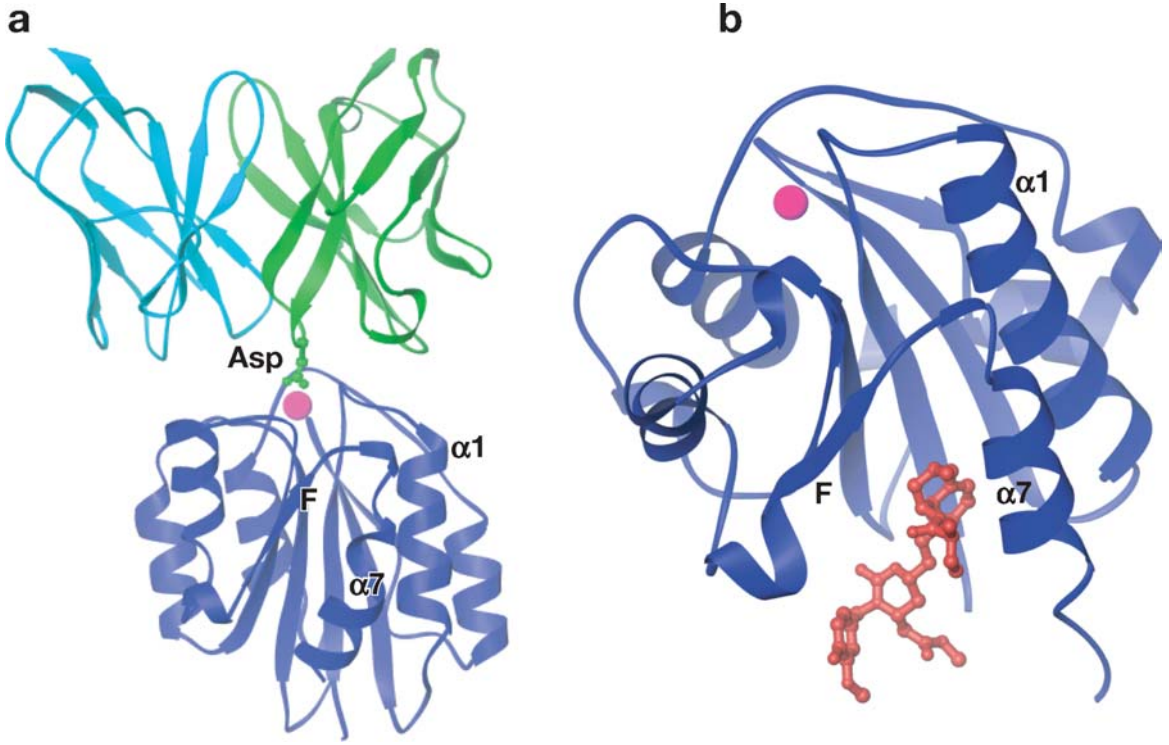

Figure 3

Structures of competitive and allosteric antagonists of αA. (*a*) Ribbon diagram of αA-Fab complex. αA is from integrin α1 (*blue*), and the antibody's variable heavy (*green*) and light (*cyan*) chains are shown. The MIDAS Mn^{2+} is the purple sphere. The sidechain of the ligand-mimetic D101, which coordinates MIDAS, is labeled, as is the F-α7 segment. (*b*) Structure of αA-lovastatin complex. Ribbon diagram drawn though the Cα positions of αA from integrin CD11a. Lovastatin (*red*) binds at a crevice between the F-strand and α7 helix (*labeled*). The MIDAS metal is the purple sphere.

molecule. This sharp bending occurs between the thigh and calf-1 domains of αV(α-genu) and approximately between EGF domains 1 and 2 of β3 (β-genu). Extension at the knees produces an integrin (**Figure 4*b***), which resembles the conventional shape of integrins derived from previous electron microscopy images, showing an elongated molecule with an oval ligand-binding head sitting on top of two extended legs (Nermut et al. 1988). A metal ion (Ca^{2+} or Mn^{2+}) occupies the α-genu in both the unliganded and liganded structures. At the base of the propeller, blades 4–7 each contain a metal ion coordinated in a β-hairpin loop, which can be occupied with Ca^{2+} or Mn^{2+}. These cations may help rigidify the propeller's interface with the thigh domain.

Heterodimer Formation

The major continuous intersubunit contact is present at the βA/propeller interface. At this interface's core is an Arg621 (a lysine in all other integrins except β8); the Arg621 protrudes from a 3_{10} helix of βA into the center of the propeller channel, and is caged into place by two rings of predominantly aromatic amino acids. The striking similarity of this interface to that which is between the Gα (an αA-like fold) and Gβ (a seven-bladed β-propeller) of G proteins suggests that this interface is likewise dynamic (Xiong et al. 2001). This core arrangement is duplicated in the binding interface of the βA domain with the propeller from integrin αIIb (Xiao et al. 2004).

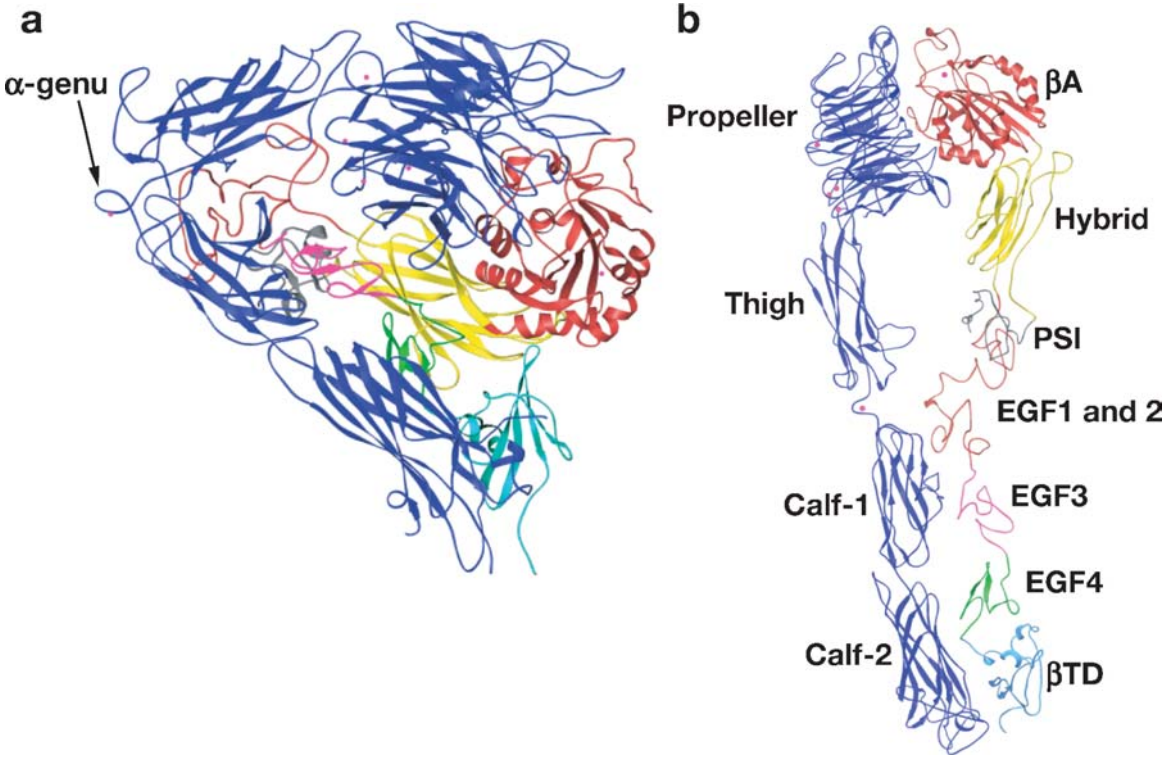

Figure 4

Structure of the integrin $\alpha V\beta 3$ ectodomain. (*a*) Ribbon diagram of the structure of the unliganded $\alpha V\beta 3$. The protein is bent at a flexible region (*α-genu*, *arrow*), occupied by a metal ion (*purple sphere*). (*b*) A genu-extended model clearly revealing the various integrin domains (*labeled*). EGF1 and EGF2 are not visible in the structure; their approximate location is indicated in gray. The four metal ions at the bottom of the propeller and the ADMIDAS ion (*all in purple*) are shown.

Additional contacts bury a surface area of about 1500 Å^2 in each integrin. Eight residues from βA [L258, D259, R261, L262 (from the 3_{10} helix), S291 and Y321, D217, and T254] contact ($\leq$3.5 Å) the αV propeller. The first six also contact αIIb in integrin αIIbβ3; in addition, R216, Lys253, S162, S168, P169, D179 (the last four from the specificity-determining loop, SDL), and E297 (from the α5 helix) contribute selectively to the βA interface with αIIb. The SDL segment may also contribute to the heterodimer interface in other integrins such as $\alpha 6\beta 1$, $\alpha V\beta 1$, and $\alpha L\beta 2$ but not $\alpha 5\beta 1$, $\alpha 4\beta 1$, $\alpha V\beta 3$, or $\alpha 6\beta 4$ (Takagi et al. 2002a). Inclusion of the β3 SDL region in the interface with αIIb (but not αV) is accounted for by the longer B2-C2 (of blade 2) and D2-A3 loops (between blades 2 and 3) of the αIIb propeller. These findings indicate that usage of subunit interface residues varies among integrins, with a variable contribution of the SDL loop to this interface.

Structures of the Unliganded and Liganded βA Domain

The structure of βA is largely superimposable onto that of αA (Xiong et al. 2003). One distinguishing feature is the presence of two insertions in βA: one that forms the core of the interface with the α-subunit's propeller domain and the second, the SDL loop, which is involved in ligand binding and also contributes to the intersubunit interface in some

integrins. A second distinguishing feature is the presence of a new cation site, ADMIDAS, which is adjacent to the MIDAS cation. The Ca^{2+} at this site is coordinated by the side chains of D126 and D127 (both from the α1 helix) and the carbonyl oxygens of MIDAS S123 (from loop 1) and of M335 (from the activation regulatory F-α7 loop) (**Figure 5*a***). The stable occupation by Ca^{2+} is in large part explained by the much higher propensity of Ca^{2+} for carbonyl coordination (Harding 2001). Thus, a novel ionic contact stabilizes the F-α7 loop in βA through linkage to the activation-sensitive top of the α1 helix and thereby replaces the largely hydrophobic contact at this site in αA domains. A third feature of βA, not found in αA, is that the unliganded $\alpha V\beta 3$ structure does not have a MIDAS cation, as the side chain of E220 (equivalent to T209 from loop 2) blocks access to MIDAS. An Mn^{2+} replaces the Ca^{2+} at ADMIDAS when the ectodomain is crystallized in the presence of this cation; this replacement was associated with very small movements in the F-α7 loop and the top of the α7 helix, which are similar in direction to those found in the liganded structure (see below). Although these movements did not alter the pattern of ADMIDAS coordination, they may have a priming effect by lowering the energy

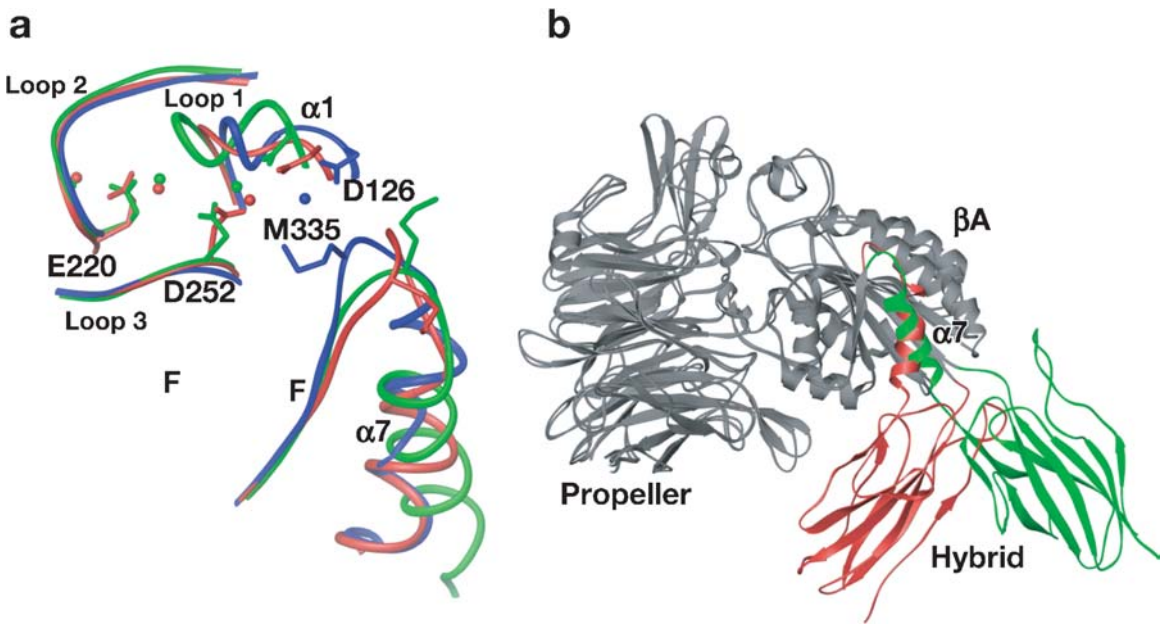

Figure 5

Structures of unliganded and liganded βA domains in the bent and legless integrins. (*a*) Ribbon diagram showing the three MIDAS loops and the side chains for key MIDAS coordinating residues in the unliganded (*blue*) and liganded (*red*) bent integrin from $\alpha V\beta 3$ and the liganded legless integrin (*green*) from $\alpha IIb\beta 3$. The side chains of two of the six ADMIDAS metal-coordinating residues M335 (from the F-α7 loop) and D126 (from α1 helix) in the three structures are shown in their respective colors, but labeled only in the unliganded one. Note that the MIDAS coordinating residues are superimposible in the two liganded structures. The unliganded structure only has the ADMIDAS metal (*blue*). All three metal ions (from left to right: LIMBS, MIDAS, ADMIDAS) are bound in both liganded structures and colored accordingly (for detailed metal coordination spheres, see Xiong et al. 2002, Xiao et al. 2004). (*b*) Ribbon diagram of the propeller, βA, and hybrid domains from the liganded bent and legless integrin forms. Non-moving parts of the Cα traces are in gray. All major moving segments from liganded bent (*red*) and liganded legless (*green*) are shown.

barrier for activation (Xiong et al. 2002). Consistently, Mn^{2+} was found to enhance ligand-binding function of an inactive form of full-length αIIbβ3 but was unable to convert this form into the active state (Yan et al. 2000).

LIMBS cation: a cation occupying a ligand-associated metal-binding site

The Integrin Ligand-Binding Site and Ligand-Associated Structural Changes

When a cyclic pentapeptide containing the prototypical ligand Arg-Gly-Asp is soaked into the Mn^{2+}-bound structure, it binds at a crevice between the propeller and the βA domains (Xiong et al. 2002). Its binding is associated with both tertiary and quaternary changes in the integrin. In the ligand-bound integrin, the ionic contact of the F-α7 loop with the α1 helix through M335 is broken, which leads to a ~2 Å inward pull of this helix as occurs with liganded αA domains, along with a large inward displacement of the ADMIDAS Mn^{2+} with the MIDAS carboxyl oxygen of D251 now replacing the carbonyl oxygen of M335. This new coordination favors the occupation of ADMIDAS with Mn^{2+} versus Ca^{2+} (**Figure 5*a***). MIDAS is now occupied by Mn^{2+}, which is coordinated in an open configuration through the D119xSxS of loop 1, directly through contact by E220 (from loop 2), and indirectly through D252 of loop 3. As in αA, the sixth metal coordination sphere is now provided by the ligand Asp, while the ligand Arg occupies a pocket in the propeller, thus bringing the propeller and βA domains closer together. The position of MIDAS is stabilized further through the repositioned ADMIDAS and by a third LIMBS cation. The LIMBS cation is coordinated by the carboxylate oxygen of E220; the side chains of D158, N215, and D217; and the carbonyl oxygens of D217 and P219 (Xiong et al. 2002). Consistent with its predicted stabilizing effect on the MIDAS metal, LIMBS has been shown to act as a positive regulator of high-affinity ligand binding (Chen et al. 2003). It has been shown (Hu et al. 1999) that β3 integrins contain two classes of ion-binding sites: a ligand-competent high-affinity site that must be occupied for the ligand to bind, most likely MIDAS; and a low-affinity Ca^{2+}-binding inhibitory (I) site, likely to be ADMIDAS, allosterically linked to the ligand-binding pocket, which increases the rate of ligand dissociation. Mn^{2+} activates integrins by competing with Ca^{2+} at the ADMIDAS. Thus, ADMIDAS appears to have a dual role in integrin function stabilizing the unliganded state (in the Ca^{2+}-bound form) as well as the liganded state (by stabilizing the MIDAS metal). This dual role may explain the discrepant data in the literature assessing the role of ADMIDAS in adhesion. In one study, disruption of ADMIDAS from integrin $\alpha4\beta7$ switched adhesion from low-affinity rolling to high-affinity firm adhesion (Chen et al. 2003). A second study, carried out in $\alpha5\beta1$, found that disrupting ADMIDAS impaired ligand binding and outside-in signaling (Mould et al. 2003a).

Four ligand- or pseudoligand-occupied crystal structures (Xiao et al. 2004) of a legless version of integrin αIIbβ3 (lacking the three leg domains of αIIb and the five leg domains of β3) have been recently determined in the absence (one form) or presence of the complex-specific and function-blocking mAb 10E5 Fab, which binds the inactive integrin (Coller et al. 1983). All four structures are stabilized by major crystal contacts at the F-α7 loop from symmetry-related molecules. There is minimal movement of the F–α7 loop but a greater inward movement of the α1 helix when compared to those of the liganded αVβ3 ectodomain structure (**Figure 5*a*,*b***). These movements had no impact on the already open MIDAS configuration found in the liganded full-length αVβ3 ectodomain (**Figure 5*a*,*b***). In the legless structure, a one-turn downward movement of the α7 helix, which also pivots laterally, is observed, in association with large swing-out motions of the hybrid domain at the hybrid-βA interface (69°, 57°, 59°, and 61° degrees in the four structures) (**Figure 5*b***). These hybrid swings, which in

the crystal structures are stabilized by a nonphysiologic salt bridge between the PSI and propeller domains of the same molecule, are associated with a smaller βA/hybrid interface (~350 Å^2 or half that in the bent state) that is contributed mainly by Y110 and Y348, and that varies slightly in the four structures. If, as it is in the αA domains, the F-α7 loop is the primary trigger in the transition from the closed to open MIDAS configuration in βA, the change in this loop seen in the liganded full-length αVβ3 ectodomain appears to have achieved this goal. The small additional movement in this loop seen in the legless form adds little to this functionality. It has been proposed (see below) that the one-turn downward and lateral movement of the α7 helix seen in the legless crystal form is necessary to transition βA to the high-affinity state and that it did not occur in the liganded full-length ectodomain of αVβ3 because of unfavorable intramolecular contacts from the leg segments. An alternative explanation is that the α7 movement in the legless structure may be induced by ligand, and mimicked in the legless structure by the introduced truncation; as noted above, the α7 helix of CD11a is highly flexible in the isolated domain but apparently not in the intact integrin.

The αA Domain Is an Endogenous Ligand of βA

Integrins are activated from inside-out whether or not they have the ligand-binding αA domain, which is a recent addition to the integrin during evolution (Whittaker & Hynes 2002). How is this achieved? αA loops out from the D3A3 loop of the propeller (between its second and third blades). In αA-lacking integrins, this loop forms part of the ligand-binding interface. αA is linked to the D3A3 loop by three residues N-terminally and 15 residues C-terminally. Function-blocking mAbs to the linker regions have been described (reviewed in Alonso et al. 2002).

Alanine or glutamine substitution of an invariant E320 (in CD11b) at the very end of the α7 helix of closed αA (which becomes disordered in the open structure) inactivates the integrin even in the presence of Mn^{2+}, whereas an aspartate substitution of this residue is better tolerated (Alonso et al. 2002). These findings indicate that the length and charge of the residue at position 320 are both important in activation of this integrin. This leads us to propose that E320 acts as an endogenous ligand linking αA to the activation-sensitive βA domain (Alonso et al. 2002). We envision that the open and closed conformations of αA exist in an equilibrium that heavily favors the closed state in the low-affinity integrin (Li et al. 1998). Inside-out activation of the βA domain allows E320 of open αA to coordinate directly the βA MIDAS metal and thus to stabilize the open state (**Figure 6**). Consistently, it was recently shown that mutating the equivalent glutamate residue in CD11a produces the same outcome (Shimaoka et al. 2003a).

A new class of antagonists that block ligand binding by interfering with this αA/βA interface have been identified (Gadek et al. 2002, Welzenbach et al. 2002). The nonstatin-derived XVA143 acts by directly coordinating the βA MIDAS metal, thus severing the αA link to βA. Binding of XVA143 induces the activation epitopes 24, KIM127 and NKI-L16; this indicates that this class acts in fact as pseudoligands, competitively inhibiting E320 or its equivalent from ligating βA and hence preventing αA from stably assuming the open state (Shimaoka et al. 2003a).

THE INTEGRIN TRANSMEMBRANE AND CYTOPLASMIC SEGMENTS

Structures of the Cytoplasmic Tails

Several NMR structures of integrin α- and/or β-subunit cytoplasmic tails were reported (Li et al. 2001, Ulmer et al. 2001, Vinogradova et al. 2002, 2004, Weljie et al. 2002). The initial studies did not agree on

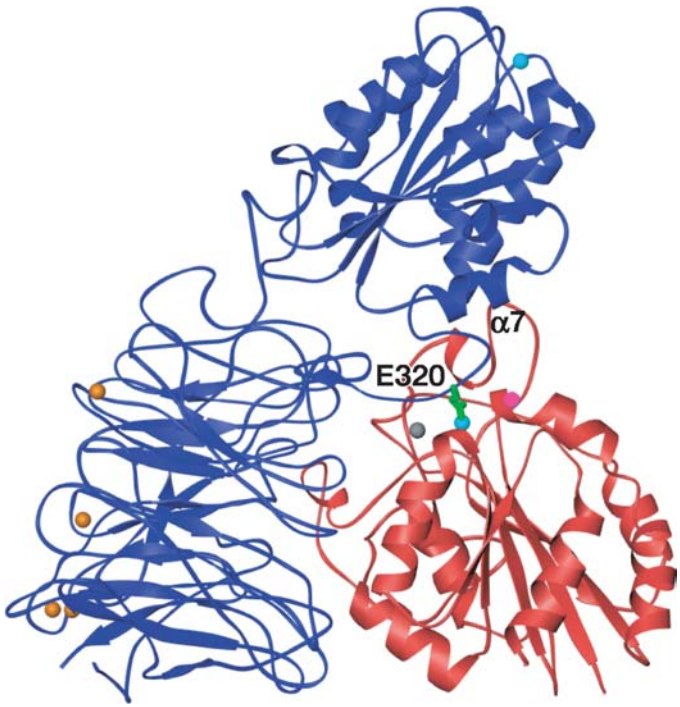

Figure 6

αA is an endogenous integrin ligand. Hypothetical model of the CD11b/CD18 head segment based on the αVβ3 and the CD11b αA crystal structures. The invariant E320 (*green side chain*) at the C terminus of the α7 helix coordinates the MIDAS ion (*cyan sphere*) of active βA, but only when the α7 helix has moved downward in open αA. The four metal ions (*orange spheres*) at the bottom of the propeller are also shown. The ADMIDAS and LIMBS ions are in magenta and gray, respectively. The αA MIDAS ion is in cyan.

whether the α and β cytoplasmic tails interacted at all. Two subsequent studies then demonstrated that such an interaction took place in the aqueous environment but disagreed on the nature of the αβ interface. Vinogradova et al. (2002), using full-length cytoplasmic tails of αIIb (K989-E1008) and β3 (K716-T762) (**Figure 7*a***), found a single population of tails thought to represent the integrin tails in the low-affinity state, where the conserved membrane-proximal regions of αIIb (K989xGFFKR995) and β3 (K716LLxxIHD723) are α-helical and interact via a combination of electrostatic (involving a salt bridge between the cytoplasmic residues R995 and D723) and hydrophobic contacts (with V990; F992 of αIIb; and L718, I719, I721, and H722 of β3 being interfacial residues). The αIIb helix terminates at P998, followed by a turn that allows the C-terminal loop to fold back and interact with the membrane-proximal region. The final 25 residues following the β3 membrane-proximal helix are disordered. Disruption of either the hydrophobic or electrostatic interaction destabilized the cytoplasmic complex, as did the addition of the cytoskeletal protein talin, a known integrin activator (Garcia-Alvarez et al. 2003). Using the synthetic αIIb and β3 peptides M987-R995 and K716-D740, Weljie et al. (2002) found evidence for two conformations. In both NMR structures, the β3 helices of each are situated on the opposite side of the αIIb N-terminal helix found by Vinogradova et al.; in this position, these helices would clash with the αIIb C-terminal segment. In one conformation, the main interhelical contact involves V990 and F993 of αIIb and I719 of β3 in addition to the R995-D723 salt bridge. In the second conformation, a bend between D723 and A728 of β3 is found, which prevents formation of the salt bridge. Weljie et al. (2002) proposed that the cytoplasmic tails remain complexed upon activation, with the β3-hinge at D723-A728 playing a central role in the switch between the low- and high-affinity states.

Significant changes in the structure of the full-length α and β cytoplasmic tails are seen in the presence of the membrane-mimetic dodecylphosphocholine (DPC) (Vinogradova et al. 2004) (**Figure 7*b***). These changes reconcile some of the structural differences observed in the two studies discussed above (Vinogradova et al. 2002 and Weljie et al. 2002). The membrane-proximal α and β segments no longer associate, as each segment is now embedded in DPC; as a result, the αIIb tail does not fold back to interact with the α-helical membrane-proximal region; thus, the predicted clash of the αIIb tail with the β3 helices in Weljie et al. (2002)'s structures may be avoided. Significantly, the disordered C-terminal segment of β3 tail is

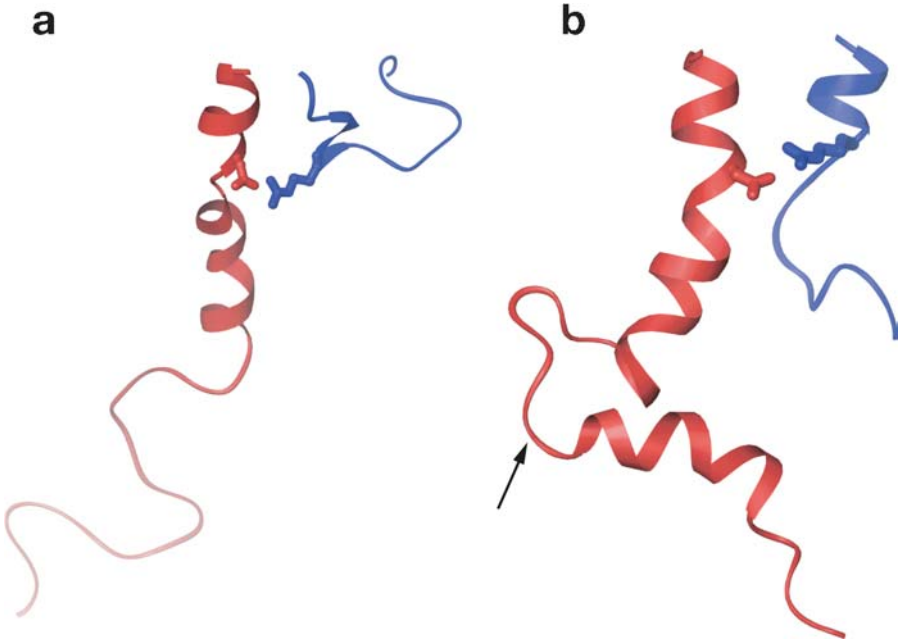

Figure 7

Structures of the αIIbβ3 cytoplasmic tails. (*a*) Ribbon diagram showing the NMR structure of the αIIb (*blue*) and β3 (*red*) tail complex. The side chains of D723 (from β3) and Arg995 (αIIb) form a salt bridge. (*b*) Structures of αIIb (*blue*) and β3 (*red*) cytoplasmic tails in detergent, where no association was detected by NMR. Note that the C-terminal portion of the β3 is now structured, with a membrane-anchoring NPxY site indicated by an arrow. We have oriented the αIIb structure so as to form the salt bridge with β3.

now ordered: the membrane-proximal α-helix (K716-R734) is followed by a flexible NPxY-containing loop and a second short helix at Y747-T755. A kink at D723 bends the long helix slightly and thus brings the flexible loop into possible contact with the membrane surface. A similar bend at this position observed in one of the two conformations in Weljie et al. (2002) may thus be reflective of the conformational space the TM segments can occupy under different conditions in the absence of the extracellular domain, which probably restricts this space. Vinogradova et al. (2004) proposed a model in which the interacting α (K989xGFF) and β (K716LLxxI) membrane-proximal regions that form in solution (and naturally within the cytoplasm) represent the low-affinity state of the integrin and the noninteracting tail structures in detergent represent the high-affinity integrin, in which these membrane-proximal regions are now intramembranous. An alternative model, however, is that the interacting α (K989xGFF) and β (K716LLxxI) membrane-proximal regions are embedded in the membrane in the low-affinity state, stabilized by the cytoplasmic R995-D723 salt bridge at their C termini and by the membrane-associated N744PxY loop. Binding of the known integrin-activator talin (Ulmer et al. 2003) detaches this loop from the membrane, breaks the salt bridge, and dissociates the membrane-proximal $\alpha\beta$ interface. This model is more consistent with recent data showing that the TM segment is shorter in the high-affinity state (see below). The mechanism of the talin-β3 interaction has been determined from crystallographic analysis of a chimeric protein containing the integrin-binding portion of talin linked to a β-cytoplasmic domain

TM: transmembrane

GpA: glycophorin A

peptide (Garcia-Alvarez et al. 2003). In the structure, the phosphotyrosine-binding (PTB) domain from the talin FERM domain binds the NPxY helical region of $\beta 3$. Talin has also been shown to bind the membrane-proximal segment of $\beta 3$, but the structural basis of this interaction remains to be determined.

Structure Models of the TM Segments

If the conserved α and βmembrane-proximal segments K989xGFF and K716LLxxI are embedded in the plasma membrane, then the TM segments will be 25–29 amino acids long—three to five amino acids longer than the typical TM segment of type I membrane proteins. Direct support that membrane-proximal segments can in fact be membrane embedded comes from glycosylation mapping studies, which suggested that, given their length, the TM segments are likely tilted or coiled inside the membrane (Armulik et al. 1999, Stefansson et al. 2004). Previous studies have also shown that either deletions involving the membrane-proximal segments [both inclusive of or limited to the R995-D723 salt bridge (Hughes et al. 1996)] or mutations that shorten the TM domains will switch integrins into high affinity (Partridge et al. 2004). Armulik et al. (1999) suggested that in response to inside-out activation, the conserved intramembranous K989 of αIIb and K716 of $\beta 3$ become cytosolic, probably in response to talin binding to the now cytoplasmic membrane-proximal K716LLxI segment. Given the hydrophobic nature of the membrane-proximal region, this transition would not be energetically costly. Since the TM borders at the outer membrane leaflet do not change in this process (Stefansson et al. 2004), the α and β TM segments shorten by three to five amino acids and may become less tilted or coiled, but do not slide past each other in a piston-like movement.

Although there is general agreement that modulation of the interhelical TM interface is necessary for inside-out activation, there is no consensus on the precise nature of this intramembranous interface or how the interface is modulated to effect activation. Several structural models of $\alpha\beta$ TM segments have been recently proposed, some based on experimental data. In a cryo-EM study of the full-length αIIb$\beta 3$, Adair and Yeager (2002) proposed that in the low-affinity state, αIIb and $\beta 3$ TM segments associate in an α-helical coiled coil (**Figure 8*a***). The αIIb$\beta 3$ TM segments were aligned using the R995-D723 salt bridge and mapped onto a right-handed coiled coil or a left-handed leucine zipper. Computational search of the conformational space of the TM domains suggested that the α and β TM segments each interact through a conserved GxxxG-like motif (Gottschalk et al. 2002) in the midsection of the TM segments, This interaction is used in GpA homodimer formation. A GpA-like crossing angle of 40° between the energetically favored right-handed helices (Li et al. 2005) brings αIIb Gly972 and Gly976 of the GxxxG motif into intimate contact with the $\beta 3$ TM domain, but does not allow formation of the membrane-proximal salt bridge; this implied to the authors that this form represented the high-affinity state. A second right-handed coiled-coil conformation inclusive of the membrane-proximal segment and associated with ~100° rotation of the α helix permitted the formation of the salt bridge and was thought to represent the low-affinity state (Gottschalk et al. 2002). Thus activation in these models involves interhelical rotation motion without complete dissociation of the $\alpha\beta$ TM complex. Using asparagine scanning throughout the TM helix of the $\beta 3$-subunit, Li et al. (2003) found that G708N and M701N mutations, both along one face of the helix, enable integrin αIIb$\beta 3$ to become active and constitutively cluster, and enhance the tendency of the TM helix to form homotrimers. This led Li et al. to conclude that homo-oligomerization plays a key role in integrin activation. Asparagine scanning of helices has the potential, however, to weaken some helix-helix associations while

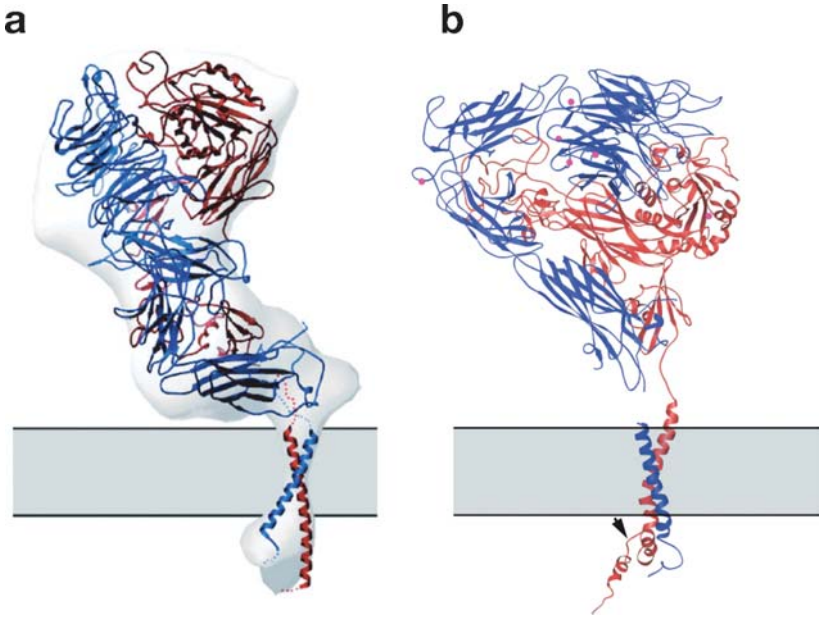

Figure 8

A hypothetical model of a membrane-bound integrin. (*a*) Ribbon model of the X-ray crystal structure of the ectodomain fitted within the map derived by electron cryomicroscopy of the full-length αIIbβ3. Hinge movements at three pivot points of the αVβ3 crystal structure (Xiong et al. 2001) were introduced to fit the map. αV- and β3-subunits are in blue and red, respectively. The map shows that the transmembrane domains are associated as a single rod of density, which has been modeled as a right-handed, parallel, α-helical coiled coil. This figure is taken from Adair & Yeager 2002 with permission. (*b*) An atomic model of a full-length β3 subunit of αVβ3. The predicted α-helical TM segments of the α- and β-subunits (Rost et al. 2004) begin with residues I966 of αIIb, V964 of αV, and I693 of β3 (based on glycation mapping) (Stefansson et al. 2004). The crystal structure of the β3-subunit from the αVβ3 ectodomain ends with G690. Further analysis of the electron density map has extended the structure to P691 (unpublished observations), which we place in the model as the first residue of the TM α helix. This placement is in view of the proline residue's propensity to stabilize strongly an α-helical conformation when placed in the first position of the helix (Senes et al. 2004). The model places the TM segment at ~45° with respect to the long axis of calf-2 domain, compared to the ~90° angle in the EM structure in *a*. The TM helix is continuous with the α-helical membrane-proximal and cytoplasmic tail of the NMR-derived structure of β3 (Vinogradova et al. 2004). Note that the proximal NPxY segment faces the membrane (*arrow*). Positioning of the αIIb TM helix in relation to that of β3 was done according to Partridge et al. (2004); this positioning allowed formation of the R995-D723 salt bridge without further modifications. The NMR structure of cytoplasmic αIIb is also from Vinogradova et al. (2004).

strengthening others (DeGrado et al. 2003); the activating effect of the G708N mutation found by Li et al. (Li et al. 2003) could thus act primarily by disrupting the $\alpha\beta$ TM helical packing and favoring homo-dimerization. In this view, homo-oligomerization, which may be favored by the GxxxG-like motifs, may be a postactivation event.

In a fourth study (Partridge et al. 2004), an unbiased random mutagenesis of the β3 TM and cytoplasmic tail identified activating point mutations in the TM segment and cytoplasmic tail but none were C-terminal to the salt bridge forming D723. A Monte Carlo simulation (Kim et al. 2003b) produced two alternative right-handed helical structures for the low-affinity state, with the TM helices packing at crossing angles either near their C or N termini. The former structure was favored by the random mutagenesis data, which

FRET: fluorescent resonance energy transfer

suggested a specific TM helix-helix packing interface in which the C-terminal β3 TM residues G708, A711, and I714 are helical contacts, with β3 G708 packing against the TM residue Thr981 of αIIb. The GxxxG-like sequences of αIIb (V971 and L974) and β3 (V700) may make some contribution to this interface but are not at its core. Finally, an in vivo cysteine cross-linking study placed the interhelical interface of the low-affinity state in the outer leaflet of the membrane (Luo et al. 2004a), in contrast to the study by Partridge et al. (2004). Treating cells with the oxidation catalyst Cu-phenanthroline improved efficiency of disulfide formation up to αIIb G972 and β3 V700 but no deeper, perhaps as a result of this catalyst's limited diffusion into the inner membrane leaflet. The proposed interhelical contact involved N-terminal residues at positions I966, W968, and G972 of αIIb; and I693, L694, V696, L697, and V700 of β3; and placed the β3 GxxxG-like (S699xxxA) motif on the opposite face of this interface, i.e., not facing the corresponding G972xxxG motif of αIIb. This interface was lost and no alternative $\alpha\beta$ disulfides or homomeric associations were detected in an activating truncating mutation of αIIb (after G991 of the KGFFKR motif or by replacing this motif with KGAAKR). The interface proposed here is largely incompatible with the one proposed by Partridge et al. (2004), since the respective core contact residues W968 and T981 are not on the same side of the helix. This may be a reflection of the limitation of such models and/or of the techniques used; for example, in vivo intramembranous cysteine cross-linking does not invariably imply that the respective cross-linked positions constitute a contact site (Homma et al. 2004). The findings from the cysteine scanning study also do not support the NMR (Weljie et al. 2002) and computational (Gottschalk et al. 2002) models in which the TM regions remain complexed in the active state. In fact, a FRET-based study, in which yellow and cyan fluorescent protein tags were fused to the C termini of the integrin α- and β-subunit cytoplasmic domains, concluded that the TM segments separate laterally in the lipid bilayer by >100 Å (Kim et al. 2003a). A lateral separation of the α- and β-transmembrane helices upon integrin activation would not likely be a fast and reversible process but energetically costly and probably slow owing to the viscosity of the plasma membrane. Although the evidence for interacting TM segments in the high-affinity state is weak at present, a reorganization of the interhelical interface in the active state through a change in tilt or rotation may be more energetically favorable and faster. It may be relevant that an inactivating disulfide is formed between αIIb G972 and β3 L697 in the active KGAAKR mutant αIIbβ3 integrin (Luo et al. 2004a); since disulfide bond formation implies a proximity of 1.9 Å or less, some components of the active integrin's TM segments appear to remain spatially close. Furthermore, if the noted disorder of the β3 C-terminal segment in the aqueous NMR structure is activation-induced, the decreased FRET observed in the GFP-tagged C termini may in part reflect this flexibility.

The Integrin Ectodomain-TM Connection: A Model Structure of the Full-Length β3-Subunit

The crystal structure of bent αVβ3 lacked the TM and cytoplasmic tails and therefore provided no information on how integrins are positioned relative to the plasma membrane. The transmembrane helices are commonly depicted as parallel to the legs; in this orientation, the ligand-binding pocket would be facing the plasma membrane and thus inaccessible to the ligand. Three-dimensional reconstruction of EM images of full-length αIIbβ3 in the low-affinity state showed, however, that the TM helices are not parallel but almost perpendicular to the long axis of the legs (**Figure 8*a***). This orientation can be readily accommodated in an atomic model of the β3-subunit inclusive of its TM and cytoplasmic segments—where

the model incorporates the NMR structure of the membrane-proximal and cytoplasmic tails of $\beta 3$ in detergent (Vinogradova et al. 2004)—and the data that suggest that a long TM segment is a feature of the inactive state (Partridge et al. 2004) (**Figure 8*b***). The modeled $\beta 3$ TM helix includes the exofacial residue D692 and extends through the membrane-proximal segment in the low-affinity state; the helix is tilted by ~35–40° to fit into the 30 Å membrane thickness. The calf-2-TM tilt angle may vary among integrins as a function of the length of their TM segments [e.g., it is 26, 22, 29, and 25 amino acids long in $\beta 1$, $\beta 8$, $\alpha 10$, and $\alpha 2$, respectively (Stefansson et al. 2004)]; the longer the TM segment, the greater the tilt angle. On the inner side of the $\beta 3$ TM helix, i.e., facing the α-subunit, are G708, A711, I714, and cytoplasmic D723, the last of which forms the salt bridge with R995. Mutations of any of these residues have been shown to activate the integrin (Partridge et al. 2004). In our model, the α-helical structure of the αIIb TM segment and its cytoplasmic tail can be accommodated in coiled-coil (Adair & Yeager 2002) or N- (Luo et al. 2004a) or C-terminal (Partridge et al. 2004) TM crossed-angle packing patterns. A C-terminal crossing based on the recent structure model of Partridge et al. (2004) is displayed in **Figure 8*b***. All three TM crossing-angles models are allowed by the presence of a five amino acid sequence linking P957, the last residue in the crystal structure of the αV ectodomain, with V964 the first TM residue.

MODELS OF INTEGRIN ACTIVATION AND SIGNALING

Inside-Out Integrin Activation

The most surprising feature of the $\alpha V\beta 3$ integrin ectodomain's crystal structure is its knee-bent conformation. Subsequent studies have confirmed that this conformation exists naturally in $\alpha V\beta 3$ as well as in other integrins. First, EM images of recombinant integrins in the presence of Ca^{2+} (Adair et al. 2005, Takagi et al. 2002b) or Mn^{2+} (Adair et al. 2005) revealed a bent form, consistent with the bent structure. Second, engineering a head-to-leg disulfide bond between the αV propeller and EGF-4 of $\beta 3$, which should lock the integrin in the bent form, led to a cell surface-expressed heterodimer (Takagi et al. 2002b). Third, clusters of monoclonal antibodies that bind to the head or membrane-proximal leg segments of native $\alpha IIb\beta 3$ on intact platelets cross-compete, consistent with the bent state of the integrin (Calzada et al. 2002). Fourth, FRET is observed between cell-bound integrins bearing fluorescent ligands and lipophilic probes, which suggests that the ligand-binding site is within ~100 Å of the lipid bilayer, consistent with a bent-integrin conformation (Chigaev et al. 2003).

It is currently thought that affinity switching is triggered intracellularly by the binding of one of two NPxY/F motifs of the integrin β cytoplasmic tail to the PTB-like F3 FERM subdomain of talin (Garcia-Alvarez et al. 2003, Yan et al. 2001): expressing talin shRNA specifically blocks binding of the activation-sensitive mAb PAC-1 to $\alpha IIb\beta 3$ in response to ADP or thrombin (Tadokoro et al. 2003). Talin shRNA-induced suppression is not reversed by activated R-Ras or the CD98 heavy chain, two previously known positive regulators of integrin activation (Tadokoro et al. 2003). Binding of talin induces spectral perturbation in the membrane-proximal region of $\beta 3$ (Li et al. 2002a, Vinogradova et al. 2002). These perturbations are prevented by the presence of the αIIb cytoplasmic tail (Ulmer et al. 2003). The role of serine/threonine and tyrosine phosphorylation of the α- and β-subunit cytoplasmic tails in this context is unclear, as is the role of RhoA, which regulates integrin affinity through a region distinct from the one that regulates avidity (Giagulli et al. 2004). Other data suggest, however, that talin-mediated activation may not be prototypic of inside-out activation of all integrins. First, down-regulation of talin by antisense mRNA or shRNA

ILK: integrin-linked kinase

reduces integrin processing and transport to the cell surface (Albiges-Rizo et al. 1995, Martel et al. 2000, 2001). Second, integrins in talin-deficient *Drosophila melanogaster* can still bind to physiologic ligands but fail to connect to the actin cytoskeleton (Brown et al. 2002, von Wichert et al. 2003). Third, $\beta 2$ integrins in resting neutrophils are linked constitutively to talin and switch to α-actinin upon activation (Sampath et al. 1998), which suggests that talin stabilizes the inactive state in this case. Fourth, the $\beta 7$ integrin binds talin poorly but binds tightly to filamin through a phosphorylation-modified ITTTI motif found between the two NPxY motifs (Calderwood et al. 2001). Even if talin is a final common pathway for activation in some integrins, its regulation and recruitment to the cell surface remains poorly understood. Currently, the only known physiologic activator of talin is PtdIns(4,5)P2 (Martel et al. 2001) produced by the action of type I PtdIns(4)P 5-kinases and regulated by PtdIns(4,5)P2 phosphatases. The type I PtdIns(4)P 5-kinases are themselves regulated by phosphatidic acid, the small G proteins Arf1 and Rho, and Src. The transience of the integrin activation response indicates the presence of downregulatory molecules as well. Independently of ERK/MAPK, H-ras suppresses integrin activation via Raf-1 (Hughes et al. 1997); this is reversed by PEA15 (phosphoprotein-enriched in astrocytes 15) (Kinbara et al. 2003). H-ras does not regulate chemokine-induced integrin activation in other cells, which suggests that the suppressive effect may be integrin-specific (Weber et al. 2001a). Other potential negative regulators of chemokine-induced activation include the serine-threonine kinase ILK (Friedrich et al. 2002) and Rac1.

The switchblade model. How are the activation events triggered inside the cell transmitted across the plasma membrane to the integrin ligand-binding site some 200 Å away? An early study, reporting the NMR structure of the recombinant EGF3 domain and a modeled EGF2 domain from the $\beta 2$-subunit, suggested that the epitope for the activation-sensitive mAb KIM127 found in EGF2/3 (Tan et al. 2000) is buried in the bent integrin structure but exposed in the knee-extended model (Beglova et al. 2002). Further, the assumption that the long axis of calf-2 is perpendicular to the plane of the plasma membrane results in an integrin in which access to the ligand-binding pocket is blocked by the membrane. The so-called switchblade model of inside-out integrin activation emerged on the basis of (*a*) additional data showing that a head-to-leg disulfide bonded integrin is inactive, and (*b*) EM two-dimensional images of the recombinant ectodomain. The latter showed mainly bent forms in 1mM Ca^{2+} changing to predominantly knee-extended, leg-separated, and wide-angled βA/hybrid forms in the presence of the activating cation Mn^{2+} with or without RGD (Takagi et al. 2002b). In the switchblade model, inside-out activation is driven by separation of the cytoplasmic and TM segments, causing a jackknife-like knee-extension of the inactive bent integrin. This extension releases the hybrid domain from its restraining interface with the leg domains, which allows the domain to swing outward and pull down the $\alpha 7$ helix of βA, thus switching βA to high affinity. Consistent with such a global conformational change, the calculated Stokes radius, based on gel elution profiles, increases from 56 Å (in 1mM Ca^{2+}) to 60 Å (in Mn^{2+}), with a further increase to 63 Å upon addition of cyclic RGD (Takagi et al. 2002b). As noted above, spatial separation of the cytoplasmic and TM segments has been demonstrated (Kim et al. 2003a). N-glycosylation sites introduced in the $\beta 1$-subunit through a P333N mutation (Luo et al. 2003a) or the better-expressed G429N (G420 in $\beta 3$) mutations (Luo et al. 2004b) are activating from a proposed wedging open of the βA/hybrid. In addition, mAb SG/19, which maintains $\alpha 5\beta 1$ in the low-affinity state, binds in 1 mM Mn^{2+} to recombinant legless integrins at the outer surface of the βA/hybrid junction (Luo et al. 2004b); it was argued that mAb

SG/19 inactivates the integrin by preventing the hybrid out-swing. Three-dimensional EM imaging of the head segment of recombinant legless $\alpha 5\beta 1$ in 1mM Ca^{2+} and 1mM Mn^{2+} yielded the acute βA/hybrid-angle form seen in the bent X-ray structure of $\alpha V\beta 3$ (Takagi et al. 2003); the absence of the wide-angled βA/hybrid form in Mn^{2+}, predominant in the two-dimensional EM structure of the complete ectodomain, is notable (Takagi et al. 2002b). A large outward swing of the hybrid domain was seen in only ~25% of the legless integrin molecules upon addition of saturating amounts of GRGDNP peptide ligand in 1 mM Ca^{2+} and in ~20% of the molecules when the physiologic ligand Fn7-10 was added in 1mM Mn^{2+} (Takagi et al. 2003); in the latter case, most FN-bound integrins displayed the wide βA/hybrid angle. Low-angle X-ray solution scattering (Mould et al. 2003c) and crystal structures of legless αIIb$\beta 3$ with small RGD-like ligands or pseudoligands (Xiao et al. 2004) all showed an outward swing of the hybrid domain of wide-ranging angles (45–80°), and the crystal structures (Xiao et al. 2004) revealed a rearranged F-$\alpha 7$ loop and a one-turn downward and outward displacement of the $\alpha 7$ helix. Disulfides introduced in the F-$\alpha 7$ region of βA of the $\beta 3$-subunit produced high- (F-strand V332C/F-$\alpha 7$ loop M335C) or low-affinity (F-strandT329C/$\alpha 7$ helix A347C) (Luo et al. 2003b, Tng et al. 2004) forms, and one-turn- ($\beta 2$-subunit residues 336–339 or 340–343) or two-turn ($\beta 2$-residues 337–343) deletions of $\alpha 7$ were also activating (Yang et al. 2004) (**Figure 9**). Furthermore, a N329S mutant in the F-$\alpha 7$ loop (equivalent to N339 in $\beta 3$), an L358A mutation in the $\alpha 7$ helix of the $\beta 1$-subunit (equivalent to I351 in the $\beta 3$-subunit and to the conserved SILEN residue I316 in αA) (Barton et al. 2004, Mould et al. 2003b) and a natural V409D of the $\alpha 7$ helix in the insect's βPS-subunit (equivalent to L341 in $\beta 3$) (Jannuzi et al. 2004) (**Figure 9**) were also activating, suggesting involvement of the F-$\alpha 7$ region in integrin activation.

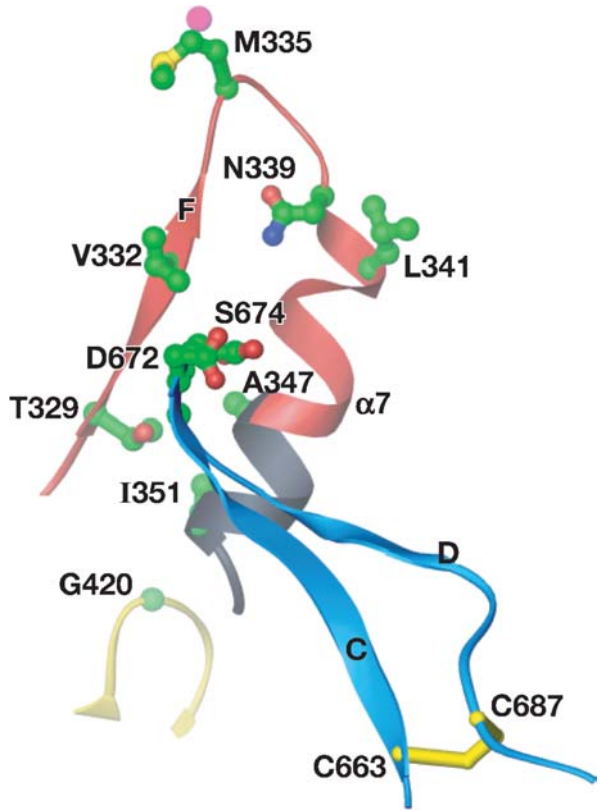

Figure 9

Activating mutations in the F-$\alpha 7$ region of βA: the deadbolt model. Ribbon diagram of the F-$\alpha 7$ region of βA (*red*). Side chains of amino acids in the F-strand, F-$\alpha 7$ loop, $\alpha 7$ helix [including the deleted segment (in *gray*)], and CD loop of the βTD are labeled; these amino acids activate the integrin when mutated. Position of the activating G420N glycan wedge mutation in the hybrid domain (*yellow*) is also shown. The CD loop interfaces with βA in a similar way to that of the competitive inhibitor lovastatin (see **Figure 3*b***), inviting the deadbolt analogy (see text for details). The cation at ADMIDAS is in magenta.

A number of other observations, however, are not consistent with knee-extension as a prerequisite for inside-out integrin activation. First, the cross-competition between clusters of monoclonal antibodies directed to the head and leg segments is retained when platelets are treated with activating agents such as ADP and thrombin (Calzada et al. 2002); this is not possible if knee-extension has taken place. Second, the complete $\alpha V\beta 3$ ectodomain, which was crystallized in 1mM Mn^{2+} in the absence (Xiong et al. 2002) or presence of cyclic RGD, assumes the bent

FN: fibronectin

uPAR: urokinase plasminogen activator receptor

conformation. Third, transmission electron microscopy and single-particle image analysis were recently used to determine the three-dimensional structure of a stable complex of the complete $\alpha V\beta 3$ ectodomain with the soluble physiologic ligand FN; this complex contains type III domains 7 to 10 and the EDB domain (FN7-EDB-10) (Adair et al. 2005). Most Mn^{2+}-bound integrin particles, whether unliganded or FN-bound, assume the compact form of the bent X-ray structure; only a rotation of the hybrid domain by ~10° with respect to that of the $\alpha V\beta 3$ X-ray structure was observed. Thus, the large outward swing of the hybrid domain is not a necessary feature of the liganded state in the complete ectodomain. Furthermore, stable binding to ligand is not associated with detectable separation of the αV- and $\beta 3$-subunit leg domains. Difference maps comparing the three-dimensional reconstructed images of the ligand-free and FN-bound $\alpha V\beta 3$ reveal density that could accommodate the RGD-containing FN10 in proximity to the ligand-binding site of $\beta 3$, with FN9 just adjacent to the synergy site–binding region of αV (**Figure 10*a***). The discrepancy of these results with those obtained earlier (Takagi et al. 2002b) may reflect in part the unbiased automatic selection routine used in the more recent study and the limitation of two-dimensional versus three-dimensional image analysis of large multidomain structures such as integrins. Fourth, the binding of the GPI-linked uPAR to cell-bound $\alpha 5\beta 1$ has been shown to stabilize interaction of the integrin with FN (Wei et al. 2005). uPAR is a small three-domain structure that binds through its N-terminal domain to blade 4 of the propeller (Simon et al. 2000); this interaction is not possible in a genuextended integrin (**Figure 10*b***). This finding also suggests that the ligand-binding site in the cell-bound bent integrin is accessible to large ligands, consistent with the modeled orientation of the integrin ectodomain described above (**Figure 8*b***). The ability of the bent integrin to bind ligands is also consistent with a number of additional observations. If the leg domains restrict the ability of the integrin to bind physiologic ligands, then removal of these domains should be activating. However, truncating the leg domains does not result in a constitutively active integrin unless induced by Mn^{2+} (Mould et al. 2003a,b). Mn^{2+}-induced activation of the legless integrin takes place in the absence of the outward swing of the hybrid domain (Takagi et al. 2003), and does not require the physical separation of the leg domains or TM segments in cell-bound integrins (Kim et al. 2003a).

How can these data be reconciled? One consideration is that the bent state is of intermediate affinity, as observed in αA domains, with high affinity achieved only in the knee-straightened conformation. However, binding to soluble physiologic ligands is a characteristic of the integrin's high- and not intermediate-affinity state (Ma et al. 2004), and the bent $\alpha V\beta 3$ ectodomain binds soluble FN. Second, the ability of the bent integrin to bind soluble FN is induced by a nonphysiologic stimulus Mn^{2+} independent of the normal inside-out activation pathway, which arguably requires the hybrid swing movement. However, the stable binding of the complete $\alpha V\beta 3$ ectodomain to soluble FN is also supported by the physiologic cation Mg^{2+} (Adair et al. 2005), consistent with the activating effect of this metal ion in various integrins (Dransfield et al. 1992). Further, 1 mM Mn^{2+} did not induce the outward hybrid swing in legless integrins unless a ligand was also present (Takagi et al. 2003). A third possibility is that the hybrid swing seen in legless integrins is an artifact resulting from truncations of the leg domains; these truncations may also result in the unstable and variable binding of FN to the recombinant legless integrin forms (Mould et al. 2003c, Takagi et al. 2003). A fourth and most likely explanation in our view is that the hybrid swing may not be a prerequisite of inside-out activation, but is ligand induced, i.e., it is a feature of outside-in signaling. The absence of the large hybrid swing in the FN-bound complete ectodomain, otherwise seen in EM and crystal

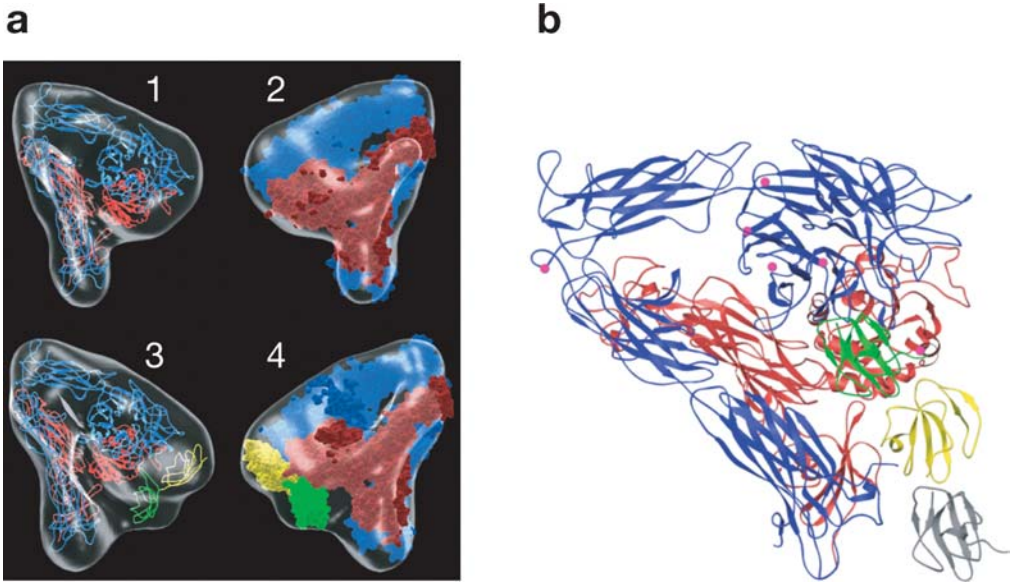

Figure 10

Ligand-binding by bent $\alpha V\beta 3$. *(a)* Pseudoatomic models of unliganded and FN-bound $\alpha V\beta 3$. αV- and $\beta 3$-subunits are in blue and red, respectively. The isosurface levels for the maps have been set to 2.6σ for each. (1) A ribbon diagram of the $\alpha V\beta 3$ crystal structure (Xiong et al. 2001) including the PSI domain (Xiong et al. 2004), fitted within the uncomplexed map. (2) The accessible surface of $\alpha V\beta 3$ (1.4 Å probe radius) fitted in the map in the same view as (1). The molecules in (2) are colored as in the ribbon models. (3) Ribbon diagram of the $\alpha V\beta 3$/FN9-10 complex fitted within the $\alpha V\beta 3$/FN7-EDB-10 map in the same orientations as (1). (4) The accessible surface model within the map viewed in the same orientation as (3). FN9 (*yellow*) and FN10 (*green*) domains are based on the X-ray structure of FN7-10 (Leahy et al. 1996) and positioned with the RGD loop of FN10 superimposed onto the cyclic RGD peptide in $\alpha V\beta 3$ (Xiong et al. 2002). This figure is modified from Adair et al. 2005 with permission. (*b*) Ribbon diagram of a hypothetical model $\alpha V\beta 3$ (colors as in *a*) in complex of the GPI-linked uPAR. The three domains of uPAR (*green*, *yellow*, and *gray*, respectively) are modeled based on the homologous CD59 domain (PDB 1CDR) (Fletcher et al. 1994). Positioning of domain 1 (*green*) of uPAR is based on mapping studies showing that this domain interacts with a short sequence in blade 4 of the propeller in proximity to the RGD-binding site. The metal ions of ADMIDAS, genu, and propeller are in magenta.

structures of the legless integrin, may reflect normal constraints by the leg domains that are overcome by binding of ligand to the intact cell-bound integrin.

The deadbolt model. So what are other potential means of achieving inside-out activation? As noted earlier, the bulk of the activating mutations in βA described to date are clustered in the F-α7 region (**Figure 9**). Such mutations include swapping the F-α7 loop residues E322LSED from the $\beta 2$-subunit with T339LSAN from $\beta 1$ (V332LSMD in $\beta 3$) (Ehirchiou et al. 2005); this mutation may act in part by disrupting the direct coordination of the ADMIDAS metal found in the unliganded state. In the crystal structure of the unliganded $\alpha V\beta 3$ ectodomain, V332 of the F-strand contacts Ser674 (~60 Å^2 contact area) from the CD loop (S673SG) of the membrane-proximal βTD. The swap of this loop with that of $\beta 2$ (G659MD) is also activating in integrin CD11b/CD18 (unpublished data). Of significance, a recent study, which systematically mutated each of the 56 cysteines in the $\beta 3$-subunit to serines, found outside the EGF domains only two among thirteen pairs that are activating (Kamata et al.

2004); one pair (C663–C687) stabilizes the CD strands of βTD (**Figure 9**). This CD strand-loop also contains epitopes for activating mAbs (Wilkins et al. 1996). Furthermore, of all the known β-subunits from sponges to humans, the βTD CD strands, inclusive of their disulfide bridge, are naturally missing in vertebrate β8. The functional implications of this deletion, if any, so far remain unexplained. This constellation of observations, unexplained by the switchblade model, has invited an alternate minimalist "deadbolt" model for inside-out activation (Xiong et al. 2003). The deadbolt model is inspired by the fact that the allosteric inhibitor lovastatin acts by binding at the F-α7 interface of the αA domain, irreversibly locking the domain in its inactive state (**Figure 3*b***). It is proposed that the novel βTD domain, through its CD loop, likewise locks βA in the low-affinity state. The deletion of the integrin TM and cytoplasmic segments (reviewed in Humphries 2000) lead to the partial disengagement of the deadbolt. This creates the priming effect that is likely the source for the weak contact observed in the ectodomain crystal structure. It is suggested that the CD loop is more engaged in the native integrin. Modifying the TM tilt angle by inside-out signals may readily and perhaps directly disengage the deadbolt (**Figure 8*b***), switching βA into the high-affinity state through restructuring of the F-α7 loop, disengaging this loop from the ADMIDAS metal and triggering the inward movement of the α1 helix. The activating mutations in the F-α7 region and the glycan wedge mutation G420N (**Figure 9**) can be reinterpreted as acting mainly by disengaging the deadbolt. The Mn^{2+}-dependent ability of the bent integrin to bind ligand in solution takes place not by leg straightening (Mould et al. 2003a) but through an Mn^{2+}-induced shift of the ADMIDAS metal coordination to that of the liganded state. This shift triggers the tertiary changes seen in the active state. The β8-subunit, with its short TM segment and a cytoplasmic tail that lacks the talin-binding site, may require the CD deletion to allow the β8 integrin heterodimer to become active, perhaps constitutively so. Transmission of inside-out activation signals across a single domain is more energetically favored, especially for a rapidly reversible reaction, in comparison with that proposed across at least five domains in the switchblade model.

Integrin Avidity

Changes in integrin avidity (clustering) complement the changes in affinity and appear critical for linking the liganded integrin to the cytoskeleton to initiate cell signaling (Hato et al. 1998). Clustering can take place in seconds when induced by chemokines and can be detected by certain mAbs such as NKI-L16 (van Kooyk et al. 1994). Integrin clustering is RhoA-dependent (Giagulli et al. 2004), and proceeds via recruitment of ζPKC to the plasma membrane, in combination with PI3K, Rap1 (Kinashi et al. 2004, Shimonaka et al. 2003), and cytohesin-1 (Weber et al. 2001b). Changes in integrin affinity are not necessarily accompanied by changes in avidity, and vice versa. For example, in T cells derived from activated Rap1 transgenic mice, integrin CD11a clusters spontaneously, but with no increase in affinity (Sebzda et al. 2002). Blockade of Src kinases or of actin polymerization prevents β2-integrin clustering without changing binding of the affinity-sensitive KIM127 mAb (Piccardoni et al. 2004). Also, inhibition of the calcium-dependent neutral protease calpain or ζPKC in leukocytes blocks clustering but not affinity modulation (Constantin et al. 2000, Giagulli et al. 2004). These findings suggest that although affinity and avidity regulation may coexist or occur sequentially, they may be driven by independent, although perhaps intersecting, pathways.

The structural basis of integrin clustering (avidity modulation) is unknown. A recent study showed that the minimal complex necessary for formation of an integrin-cytoskeleton complex is a trimer of the fibronectin's integrin-binding domain

FNIII7-10 (Jiang et al. 2003). Another study proposed that integrin clustering is the result of the TM domain–mediated homo-oligomerization (Li et al. 2003). This structure model is based on observations made with integrin TM and cytoplasmic fragments that formed dimers and trimers in sodium dodecyl sulfate or dodecylphosphocholine detergent micelles (Li et al. 2003). Full-length integrin heterodimers do not form in these same detergents, however, which suggests that alternative models of integrin clustering likely exist and remain to be discovered.

Outside-In Signaling

Extracellular ligand-bound integrins transduce a variety of signals that modulate many cellular processes, including adhesion, migration, and differentiation. Integrin-mediated signaling induces dramatic changes in the organization of the cytoskeleton (see Ridley et al. 2003 for a recent review). How are these signals transduced from the outside-in? Here, the switchblade model may provide one answer. Ligand binding to the cell-bound integrin may drive the outward hybrid swing, leg domain separation, and separation of the TM and cytoplasmic segments, inviting new interactions with cytoplasmic tails that result in the assembly of cytoskeletal-based signaling complexes. A second, although not mutually exclusive, possibility is that extracellular ligand binding triggers outside-in signaling through *cis*-interactions between integrin ectodomains and/or with other cell-surface moieties such as members of the tetraspanin protein family (Hemler 2003). As integrins transmit not only chemical but also mechanical stress signals, the flexible integrin knees may be necessary for adhesion strengthening, especially in contractile tissues.

CONCLUDING REMARKS

Spurred by the atomic resolution of the integrin ectodomain, valuable insight into the inner working of integrins has been provided to date. The new structures have explained volumes of biochemical observations but, as expected, they also raise new questions. As shown here, such questions are many. How can integrins rapidly and reversibly become activated? Do their TM segments become shorter or longer with activation? What is the nature of the TM interface and does activation require physical separation or just realignment of the TM interface? What is the structural basis of clustering? What is the nature of the moieties that maintain the cytoplasmic tails in the inactive state and how do talin and likely additional proteins modulate the structure of the C-tails to activate? How is outside-in signaling channeled and how is it translated into different cellular responses? Last but not least, what is the nature of multimolecular assemblies that mediate adhesion signaling? Answering even some of these questions will keep many busy for a long while.

ACKNOWLEDGMENTS

We thank the National Institutes of Health for grant support (DK48549, DK50305, and HL70219).

LITERATURE CITED

Adair BD, Xiong J-P, Maddock C, Goodman SL, Arnaout MA, Yeager M. 2005. Three-dimensional EM structure of the ectodomain of integrin $\alpha V\beta 3$ in a complex with fibronectin. *J. Cell Biol.* 168:1109–18

Adair BD, Yeager M. 2002. Three-dimensional model of the human platelet integrin alpha IIbbeta 3 based on electron cryomicroscopy and x-ray crystallography. *Proc. Natl. Acad. Sci. USA* 99:14059–64

Ajroud K, Sugimori T, Goldmann WH, Fathallah DF, Xiong JP, Arnaout MA. 2004. Binding affinity of metal ions to the CD11b A-domain is regulated by integrin activation and ligand. *J. Biol. Chem.* 279:25483–88

Albiges-Rizo C, Frachet P, Block MR. 1995. Down regulation of talin alters cell adhesion and the processing of the alpha 5 beta 1 integrin. *J. Cell Sci.* 108(Pt. 10):3317–29

Alonso JL, Essafi M, Xiong JP, Stehle T, Arnaout MA. 2002. Does the integrin alphaA domain act as a ligand for its betaA domain? *Curr. Biol.* 12:R340–42

Armulik A, Nilsson I, von Heijne G, Johansson S. 1999. Determination of the border between the transmembrane and cytoplasmic domains of human integrin subunits. *J. Biol. Chem.* 274:37030–34

Barton SJ, Travis MA, Askari JA, Buckley PA, Craig SE, et al. 2004. Novel activating and inactivating mutations in the integrin beta1 subunit A domain. *Biochem. J.* 380:401–7

Bhatia SK, King MR, Hammer DA. 2003. The state diagram for cell adhesion mediated by two receptors. *Biophys. J.* 84:2671–90

Beglova N, Blacklow SC, Takagi J, Springer TA. 2002. Cysteine-rich module structure reveals a fulcrum for integrin rearrangement upon activation. *Nat. Struct. Biol.* 9:282–87

Brown NH, Gregory SL, Rickoll WL, Fessler LI, Prout M, et al. 2002. Talin is essential for integrin function in Drosophila. *Dev. Cell* 3:569–79

Calderwood DA, Huttenlocher A, Kiosses WB, Rose DM, Woodside DG, et al. 2001. Increased filamin binding to beta-integrin cytoplasmic domains inhibits cell migration. *Nat. Cell Biol.* 3:1060–68

Calzada MJ, Alvarez MV, Gonzalez-Rodriguez J. 2002. Agonist-specific structural rearrangements of integrin alpha IIbbeta 3. Confirmation of the bent conformation in platelets at rest and after activation. *J. Biol. Chem.* 277:39899–908

Carson M. 1987. Ribbon models of macromolecules. *J. Mol. Graph.* 5:103–6

Chen J, Salas A, Springer TA. 2003. Bistable regulation of integrin adhesiveness by a bipolar metal ion cluster. *Nat. Struct. Biol.* 10:995–1001

Chigaev A, Blenc AM, Braaten JV, Kumaraswamy N, Kepley CL, et al. 2001. Real time analysis of the affinity regulation of alpha 4-integrin. The physiologically activated receptor is intermediate in affinity between resting and Mn(2+) or antibody activation. *J. Biol. Chem.* 276:48670–78

Chigaev A, Buranda T, Dwyer DC, Prossnitz ER, Sklar LA. 2003. FRET detection of cellular alpha4-integrin conformational activation. *Biophys. J.* 85:3951–62

Coller BS, Peerschke EI, Scudder LE, Sullivan CA. 1983. A murine monoclonal antibody that completely blocks the binding of fibrinogen to platelets produces a thrombasthenic-like state in normal platelets and binds to glycoproteins IIb and/or IIIa. *J. Clin. Invest.* 72:325–38

Constantin G, Majeed M, Giagulli C, Piccio L, Kim JY, et al. 2000. Chemokines trigger immediate beta2 integrin affinity and mobility changes: differential regulation and roles in lymphocyte arrest under flow. *Immunity* 13:759–69

DeGrado WF, Gratkowski H, Lear JD. 2003. How do helix-helix interactions help determine the folds of membrane proteins? Perspectives from the study of homo-oligomeric helical bundles. *Protein Sci.* 12:647–65

Dransfield I, Cabanas C, Craig A, Hogg N. 1992. Divalent cation regulation of the function of the leukocyte integrin LFA-1. *J. Cell Biol.* 116:219–26

Ehirchiou D, Xiong YM, Li Y, Brew S, Zhang L. 2005. Dual function for a unique site within the {beta2}I domain of integrin {alpha}M{beta}2. *J. Biol. Chem.* 280:8324–31

Emsley J, Knight CG, Farndale RW, Barnes MJ, Liddington RC. 2000. Structural basis of collagen recognition by integrin alpha2beta1. *Cell* 101:47–56

Fletcher CM, Harrison RA, Lachmann PJ, Neuhaus D. 1994. Structure of a soluble, glycosylated form of the human complement regulatory protein CD59. *Structure* 2:185–99

Friedrich EB, Sinha S, Li L, Dedhar S, Force T, et al. 2002. Role of integrin-linked kinase in leukocyte recruitment. *J. Biol. Chem.* 277:16371–75

Gadek TR, Burdick DJ, McDowell RS, Stanley MS, Marsters JC Jr, et al. 2002. Generation of an LFA-1 antagonist by the transfer of the ICAM-1 immunoregulatory epitope to a small molecule. *Science* 295:1086–89

Garcia-Alvarez B, de Pereda JM, Calderwood DA, Ulmer TS, Critchley D, et al. 2003. Structural determinants of integrin recognition by talin. *Mol. Cell* 11:49–58

Giagulli C, Scarpini E, Ottoboni L, Narumiya S, Butcher EC, et al. 2004. RhoA and zeta PKC control distinct modalities of LFA-1 activation by chemokines: critical role of LFA-1 affinity triggering in lymphocyte in vivo homing. *Immunity* 20:25–35

Gottschalk KE, Adams PD, Brunger AT, Kessler H. 2002. Transmembrane signal transduction of the alpha(IIb)beta(3) integrin. *Protein Sci.* 11:1800–12

Harding MM. 2001. Geometry of metal-ligand interactions in proteins. *Acta Crystallogr. D* 57:401–11

Hato T, Pampori N, Shattil SJ. 1998. Complementary roles for receptor clustering and conformational change in the adhesive and signaling functions of integrin alphaIIb beta3. *J. Cell Biol.* 141:1685–95

Hemler ME. 2003. Tetraspanin proteins mediate cellular penetration, invasion, and fusion events and define a novel type of membrane microdomain. *Annu. Rev. Cell Dev. Biol.* 19:397–422

Homma M, Shiomi D, Kawagishi I. 2004. Attractant binding alters arrangement of chemoreceptor dimers within its cluster at a cell pole. *Proc. Natl. Acad. Sci. USA* 101:3462–67

Hu DD, White CA, Panzer-Knodle S, Page JD, Nicholson N, Smith JW. 1999. A new model of dual interacting ligand binding sites on integrin alphaIIbbeta3. *J. Biol. Chem.* 274:4633–39

Hughes PE, Diaz-Gonzalez F, Leong L, Wu C, McDonald JA, et al. 1996. Breaking the integrin hinge. *J. Biol. Chem.* 271:6571–74

Hughes PE, Renshaw MW, Pfaff M, Forsyth J, Keivens KM, et al. 1997. Suppression of integrin activation: A novel function of a Ras/Raf-initiated MAP kinase pathway. *Cell* 88:521–30

Humphries MJ. 2000. Integrin structure. *Biochem. Soc. Trans.* 28:311–39

Ingber DE. 2003. Mechanosensation through integrins: cells act locally but think globally. *Proc. Natl. Acad. Sci. USA* 100:1472–74

Jannuzi AL, Bunch TA, West RF, Brower DL. 2004. Identification of integrin beta subunit mutations that alter heterodimer function in situ. *Mol. Biol. Cell* 15:3829–40

Jiang G, Giannone G, Critchley DR, Fukumoto E, Sheetz MP. 2003. Two-piconewton slip bond between fibronectin and the cytoskeleton depends on talin. *Nature* 424:334–37

Kallen J, Welzenbach K, Ramage P, Geyl D, Kriwacki R, et al. 1999. Structural basis for LFA-1 inhibition upon lovastatin binding to the CD11a I-domain. *J. Mol. Biol.* 292:1–9

Kamata T, Ambo H, Puzon-McLaughlin W, Tieu KK, Handa M, et al. 2004. Critical cysteine residues for regulation of integrin alphaIIbbeta3 are clustered in the epidermal growth factor domains of the beta3 subunit. *Biochem. J.* 378:1079–82

Karpusas M, Ferrant J, Weinreb PH, Carmillo A, Taylor FR, Garber EA. 2003. Crystal structure of the alpha1beta1 integrin I domain in complex with an antibody Fab fragment. *J. Mol. Biol.* 327:1031–41

Kim M, Carman CV, Springer TA. 2003a. Bidirectional transmembrane signaling by cytoplasmic domain separation in integrins. *Science* 301:1720–25

Kim M, Carman CV, Yang W, Salas A, Springer TA. 2004. The primacy of affinity over clustering in regulation of adhesiveness of the integrin {alpha}L{beta}2. *J. Cell Biol.* 167:1241–53

Kim S, Chamberlain AK, Bowie JU. 2003b. A simple method for modeling transmembrane helix oligomers. *J. Mol. Biol.* 329:831–40

Kinashi T, Aker M, Sokolovsky-Eisenberg M, Grabovsky V, Tanaka C, et al. 2004. LAD-III, a leukocyte adhesion deficiency syndrome associated with defective Rap1 activation and impaired stabilization of integrin bonds. *Blood* 103:1033–36

Kinbara K, Goldfinger LE, Hansen M, Chou FL, Ginsberg MH. 2003. Ras GTPases: integrins' friends or foes? *Nat. Rev. Mol. Cell Biol.* 4:767–76

Leahy DJ, Aukhil I, Erickson HP. 1996. 2.0 A crystal structure of a four-domain segment of human fibronectin encompassing the RGD loop and synergy region. *Cell* 84:155–64

Lee J-O, Bankston LA, Arnaout MA, Liddington RC. 1995a. Two conformations of the integrin A-domain (I-domain): a pathway for activation? *Structure* 3:1333–40

Lee J-O, Rieu P, Arnaout MA, Liddington R. 1995b. Crystal structure of the A-domain from the α-subunit of $\beta 2$ integrin complement receptor type 3 (CR3, CD11b/CD18). *Cell* 80:631–38

Li R, Babu CR, Lear JD, Wand AJ, Bennett JS, DeGrado WF. 2001. Oligomerization of the integrin alphaIIbbeta3: roles of the transmembrane and cytoplasmic domains. *Proc. Natl. Acad. Sci. USA* 98:12462–67

Li R, Babu CR, Valentine K, Lear JD, Wand AJ, et al. 2002a. Characterization of the monomeric form of the transmembrane and cytoplasmic domains of the integrin beta 3 subunit by NMR spectroscopy. *Biochemistry* 41:15618–24

Li R, Haruta I, Rieu P, Sugimori T, Xiong JP, Arnaout MA. 2002b. Characterization of a conformationally sensitive murine monoclonal antibody directed to the metal ion-dependent adhesion site face of integrin CD11b. *J. Immunol.* 168:1219–25

Li R, Mitra N, Gratkowski H, Vilaire G, Litvinov R, et al. 2003. Activation of integrin alphaI-Ibbeta3 by modulation of transmembrane helix associations. *Science* 300:795–98

Li R, Rieu P, Griffith DL, Scott D, Arnaout MA. 1998. Two functional states of the CD11b A-domain: correlations with key features of two Mn2+-complexed crystal structures. *J. Cell Biol.* 143:1523–34

Li W, Metcalf DG, Gorelik R, Li R, Mitra N, et al. 2005. A push-pull mechanism for regulating integrin function. *Proc. Natl. Acad. Sci. USA* 102:1424–29

Litvinov RI, Shuman H, Bennett JS, Weisel JW. 2002. Binding strength and activation state of single fibrinogen-integrin pairs on living cells. *Proc. Natl. Acad. Sci. USA* 99:7426–31

Lollo BA, Chan KWH, Hanson EM, Moy VT, Brian AA. 1993. Direct evidence for two affinity states for lymphocyte function-associated antigen 1 on activated T cells. *J. Biol. Chem.* 268:21693–700

Lu G. 2000. TOP: A new method for protein structure comparisons and similarity searches. *J. Appl. Cryst.* 33:176–83

Lupher ML Jr, Harris EA, Beals CR, Sui LM, Liddington RC, Staunton DE. 2001. Cellular activation of leukocyte function-associated antigen-1 and its affinity are regulated at the I domain allosteric site. *J. Immunol.* 167:1431–39

Luo BH, Springer TA, Takagi J. 2003a. Stabilizing the open conformation of the integrin headpiece with a glycan wedge increases affinity for ligand. *Proc. Natl. Acad. Sci. USA* 100:2403–8

Luo BH, Springer TA, Takagi J. 2004a. A specific interface between integrin transmembrane helices and affinity for ligand. *PLoS Biol.* 2:e153

Luo BH, Strokovich K, Walz T, Springer TA, Takagi J. 2004b. Allosteric beta1 integrin antibodies that stabilize the low affinity state by preventing the swing-out of the hybrid domain. *J. Biol. Chem.* 279:27466–71

Luo BH, Takagi J, Springer TA. 2003b. Locking the beta 3 integrin I-like domain into high and low affinity conformations with disulfides. *J. Biol. Chem.* 279:10215–21

Ma YQ, Plow EF, Geng JG. 2004. P-selectin binding to P-selectin glycoprotein ligand-1 induces an intermediate state of alphaMbeta2 activation and acts cooperatively with extracellular stimuli to support maximal adhesion of human neutrophils. *Blood* 104:2549–56

Martel V, Racaud-Sultan C, Dupe S, Marie C, Paulhe F, et al. 2001. Conformation, localization, and integrin binding of talin depend on its interaction with phosphoinositides. *J. Biol. Chem.* 276:21217–27

Martel V, Vignoud L, Dupe S, Frachet P, Block MR, Albiges-Rizo C. 2000. Talin controls the exit of the integrin alpha 5 beta 1 from an early compartment of the secretory pathway. *J. Cell Sci.* 113(Pt. 11):1951–61

McCleverty CJ, Liddington RC. 2003. Engineered allosteric mutants of the integrin alphaM-beta2 I domain: structural and functional studies. *Biochem. J.* 372:121–27

Michishita M, Videm V, Arnaout MA. 1993. A novel divalent cation-binding site in the A domain of the beta 2 integrin CR3 (CD11b/CD18) is essential for ligand binding. *Cell* 72:857–67

Mould AP, Barton SJ, Askari JA, Craig SE, Humphries MJ. 2003a. Role of ADMIDAS cation-binding site in ligand recognition by integrin {alpha}5{beta}1. *J. Biol. Chem.* 278:51622–29

Mould AP, Barton SJ, Askari JA, McEwan PA, Buckley PA, et al. 2003b. Conformational changes in the integrin beta A domain provide a mechanism for signal transduction via hybrid domain movement. *J. Biol. Chem.* 278:17028–35

Mould AP, Symonds EJ, Buckley PA, Grossmann JG, McEwan PA, et al. 2003c. Structure of an integrin-ligand complex deduced from solution x-ray scattering and site-directed mutagenesis. *J. Biol. Chem.* 278:39993–99

Nermut MV, Green NM, Eason P, Yamada SS, Yamada KM. 1988. Electron microscopy and structural model of human fibronectin receptor. *EMBO J.* 7:4093–99

Partridge AW, Liu S, Kim S, Bowie JU, Ginsberg MH. 2004. Transmembrane domain helix packing stabilizes integrin alpha IIbbeta 3 in the low affinity state. *J. Biol. Chem.* 280:7294–300

Piccardoni P, Manarini S, Federico L, Bagoly Z, Pecce R, et al. 2004. SRC-dependent outside-in signaling is a key step in the process of auto-regulation of beta2 integrins in polymorphonuclear leukocytes. *Biochem J.* 380(Pt. 1):57–65

Qu A, Leahy DJ. 1995. Crystal structure of the I-domain from the CD11a/CD18 (LFA-1, $\alpha L\beta 2$) integrin. *Proc. Natl. Acad. Sci.* 92:10277–81

Qu A, Leahy DJ. 1996. The role of the divalent cation in the structure of the I domain from the CD11a/CD18 integrin. *Structure* 4:931–42

Ridley AJ. 2004. Pulling back to move forward. *Cell* 116:357–58

Ridley AJ, Schwartz MA, Burridge K, Firtel RA, Ginsberg MH, et al. 2003. Cell migration: integrating signals from front to back. *Science* 302:1704–9

Rieu P, Sugimori T, Griffith DL, Arnaout MA. 1996. Solvent accessible residues on the MIDAS face of integrin CR3 mediate its binding to the neutrophil adhesion inhibitor NIF. *J. Biol. Chem.* 271:15858–61

Rost B, Yachdav G, Liu J. 2004. The PredictProtein server. *Nucleic Acids Res.* 32:W321–26

Sampath R, Gallagher PJ, Pavalko FM. 1998. Cytoskeletal interactions with the leukocyte integrin beta2 cytoplasmic tail. Activation-dependent regulation of associations with talin and alpha-actinin. *J. Biol. Chem.* 273:33588–94

Schwartz MA, Ginsberg MH. 2002. Networks and crosstalk: integrin signalling spreads. *Nat. Cell Biol.* 4:E65–68

Sebzda E, Bracke M, Tugal T, Hogg N, Cantrell DA. 2002. Rap1A positively regulates T cells via integrin activation rather than inhibiting lymphocyte signaling. *Nat. Immunol.* 3:251–58

Senes A, Engel DE, DeGrado WF. 2004. Folding of helical membrane proteins: the role of polar, GxxxG-like and proline motifs. *Curr. Opin. Struct. Biol.* 14:465–79

Shimaoka M, Salas A, Yang W, Weitz-Schmidt G, Springer TA. 2003a. Small molecule integrin antagonists that bind to the beta2 subunit I-like domain and activate signals in one direction and block them in the other. *Immunity* 19:391–402

Shimaoka M, Xiao T, Liu JH, Yang Y, Dong Y, et al. 2003b. Structures of the alphaL I domain and its complex with ICAM-1 reveal a shape-shifting pathway for integrin regulation. *Cell* 112:99–111

Shimonaka M, Katagiri K, Nakayama T, Fujita N, Tsuruo T, et al. 2003. Rap1 translates chemokine signals to integrin activation, cell polarization, and motility across vascular endothelium under flow. *J. Cell Biol.* 161:417–27

Simon DI, Wei Y, Zhang L, Rao NK, Xu H, et al. 2000. Identification of a urokinase receptor-integrin interaction site. Promiscuous regulator of integrin function. *J. Biol. Chem.* 275:10228–34

Smith MJ, Berg EL, Lawrence MB. 1999. A direct comparison of selectin-mediated transient, adhesive events using high temporal resolution. *Biophys. J.* 77:3371–83

Springer TA. 1997. Folding of the N-terminal, ligand-binding region of integrin alpha-subunits into a beta-propeller domain. *Proc. Natl. Acad. Sci. USA* 94:65–72

Stefansson A, Armulik A, Nilsson I, von Heijne G, Johansson S. 2004. Determination of N- and C-terminal borders of the transmembrane domain of integrin subunits. *J. Biol. Chem.* 279:21200–5

Tadokoro S, Shattil SJ, Eto K, Tai V, Liddington RC, et al. 2003. Talin binding to integrin beta tails: a final common step in integrin activation. *Science* 302:103–6

Takagi J, DeBottis DP, Erickson HP, Springer TA. 2002a. The role of the specificity-determining loop of the integrin beta subunit I-like domain in autonomous expression, association with the alpha subunit, and ligand binding. *Biochemistry* 41:4339–47

Takagi J, Petre BM, Walz T, Springer TA. 2002b. Global conformational rearrangements in integrin extracellular domains in outside-in and inside-out signaling. *Cell* 110:599–11

Takagi J, Strokovich K, Springer TA, Walz T. 2003. Structure of integrin alpha5beta1 in complex with fibronectin. *EMBO J.* 22:4607–15

Tan SM, Hyland RH, Al-Shamkhani A, Douglass WA, Shaw JM, Law SK. 2000. Effect of integrin beta 2 subunit truncations on LFA-1 (CD11a/CD18) and Mac-1 (CD11b/CD18) assembly, surface expression, and function. *J. Immunol.* 165:2574–81

Tng E, Tan SM, Ranganathan S, Cheng M, Law SK. 2004. The integrin alpha L beta 2 hybrid domain serves as a link for the propagation of activation signal from its stalk regions to the I-like domain. *J. Biol. Chem.* 279:54334–39

Ulmer TS, Calderwood DA, Ginsberg MH, Campbell ID. 2003. Domain-specific interactions of talin with the membrane-proximal region of the integrin beta3 subunit. *Biochemistry* 42:8307–12

Ulmer TS, Yaspan B, Ginsberg MH, Campbell ID. 2001. NMR analysis of structure and dynamics of the cytosolic tails of integrin alpha IIb beta 3 in aqueous solution. *Biochemistry* 40:7498–508

van Kooyk Y, Weder P, Heiji K, Figdor CG. 1994. Extracellular Ca^{2+} modulates leukocyte function-associated antigen-1 cell surface distribution on T lymphocytes and consequently affects cell adhesion. *J. Cell Biol.* 124:1061–70

Vinogradova O, Vaynberg J, Kong X, Haas TA, Plow EF, Qin J. 2004. Membrane-mediated structural transitions at the cytoplasmic face during integrin activation. *Proc. Natl. Acad. Sci. USA* 101:4094–99

Vinogradova O, Velyvis A, Velyviene A, Hu B, Haas T, et al. 2002. A structural mechanism of integrin alpha(IIb)beta(3) "inside-out" activation as regulated by its cytoplasmic face. *Cell* 110:587–97

von Wichert G, Haimovich B, Feng GS, Sheetz MP. 2003. Force-dependent integrin-cytoskeleton linkage formation requires downregulation of focal complex dynamics by Shp2. *EMBO J.* 22:5023–35

Vorup-Jensen T, Ostermeier C, Shimaoka M, Hommel U, Springer TA. 2003. Structure and allosteric regulation of the alpha X beta 2 integrin I domain. *Proc. Natl. Acad. Sci. USA* 100:1873–78

Weber KS, Ostermann G, Zernecke A, Schroder A, Klickstein LB, Weber C. 2001a. Dual role of H-Ras in regulation of lymphocyte function antigen-1 activity by stromal cell-derived factor-1alpha: implications for leukocyte transmigration. *Mol. Biol. Cell* 12:3074–86

Weber KS, Weber C, Ostermann G, Dierks H, Nagel W, Kolanus W. 2001b. Cytohesin-1 is a dynamic regulator of distinct LFA-1 functions in leukocyte arrest and transmigration triggered by chemokines. *Curr. Biol.* 11:1969–74

Wei Y, Czekay RP, Robillard L, Kugler MC, Zhang F, et al. 2005. Regulation of alpha5beta1 integrin conformation and function by urokinase receptor binding. *J. Cell Biol.* 168:501–11

Weitz-Schmidt G, Welzenbach K, Dawson J, Kallen J. 2004. Improved lymphocyte function-associated antigen-1 (LFA-1) inhibition by statin derivatives: molecular basis determined by x-ray analysis and monitoring of LFA-1 conformational changes in vitro and ex vivo. *J. Biol. Chem.* 279:46764–71

Weljie AM, Hwang PM, Vogel HJ. 2002. Solution structures of the cytoplasmic tail complex from platelet integrin alpha IIb- and beta 3-subunits. *Proc. Natl. Acad. Sci. USA* 99:5878–83

Welzenbach K, Hommel U, Weitz-Schmidt G. 2002. Small molecule inhibitors induce conformational changes in the I domain and the I-like domain of lymphocyte function-associated antigen-1. Molecular insights into integrin inhibition. *J. Biol. Chem.* 277:10590–98

Whittaker CA, Hynes RO. 2002. Distribution and evolution of von Willebrand/integrin A domains: widely dispersed domains with roles in cell adhesion and elsewhere. *Mol. Biol. Cell* 13:3369–87

Wilkins JA, Li A, Ni H, Stupack DG, Shen C. 1996. Control of beta1 integrin function. Localization of stimulatory epitopes. *J. Biol. Chem.* 271:3046–51

Xiao T, Takagi J, Coller BS, Wang JH, Springer TA. 2004. Structural basis for allostery in integrins and binding to fibrinogen-mimetic therapeutics. *Nature* 432:59–67

Xiong JP, Li R, Essafi M, Stehle T, Arnaout MA. 2000. An isoleucine-based allosteric switch controls affinity and shape shifting in integrin CD11b A-domain. *J. Biol. Chem.* 275:38762–67

Xiong JP, Stehle T, Diefenbach B, Zhang R, Dunker R, et al. 2001. Crystal structure of the extracellular segment of integrin alpha Vbeta3. *Science* 294:339–45

Xiong JP, Stehle T, Goodman SL, Arnaout MA. 2003. New insights into the structural basis of integrin activation. *Blood* 102:1155–59

Xiong JP, Stehle T, Goodman SL, Arnaout MA. 2004. A novel adaptation of the integrin PSI domain revealed from its crystal structure. *J. Biol. Chem.* 279:40252–54

Xiong JP, Stehle T, Zhang R, Joachimiak A, Frech M, et al. 2002. Crystal structure of the extracellular segment of integrin alpha Vbeta3 in complex with an Arg-Gly-Asp ligand. *Science* 296:151–55

Yan B, Calderwood DA, Yaspan B, Ginsberg MH. 2001. Calpain cleavage promotes talin binding to the beta 3 integrin cytoplasmic domain. *J. Biol. Chem.* 276:28164–70

Yan B, Hu DD, Knowles SK, Smith JW. 2000. Probing chemical and conformational differences in the resting and active conformers of platelet integrin alpha(IIb)beta(3). *J. Biol. Chem.* 275:7249–60

Yang W, Shimaoka M, Chen J, Springer TA. 2004. Activation of integrin beta-subunit I-like domains by one-turn C-terminal alpha-helix deletions. *Proc. Natl. Acad. Sci. USA* 101:2333–38

Zhang L, Plow EF. 1999. Amino acid sequences within the alpha subunit of integrin alpha M beta 2 (Mac-1) critical for specific recognition of C3bi. *Biochemistry* 38:8064–71

Zhang X, Wojcikiewicz E, Moy VT. 2002. Force spectroscopy of the leukocyte function-associated antigen-1/intercellular adhesion molecule-1 interaction. *Biophys. J.* 83:2270–79

Zwartz G, Chigaev A, Foutz T, Larson RS, Posner R, Sklar LA. 2004a. Relationship between molecular and cellular dissociation rates for VLA-4/VCAM-1 interaction in the absence of shear stress. *Biophys. J.* 86:1243–52

Zwartz GJ, Chigaev A, Dwyer DC, Foutz TD, Edwards BS, Sklar LA. 2004b. Real-time analysis of very late antigen-4 affinity modulation by shear. *J. Biol. Chem.* 279:38277–86

Annual Review of Cell and Developmental Biology

Volume 21, 2005

Contents

INDEXES

ERRATA

An online log of corrections to *Annual Review of Cell and Developmental Biology* chapters may be found at http://cellbio.annualreviews.org/errata.shtml